ROYAL SOCIETY OF CHEMISTRY

REVIEW

Check for updates

Bespoke nanostars: synthetic strategies, tactics, and uses of tailored branched gold nanoparticles

Asher L. Siegel [ID] and Gary A. Baker [ID] *

Interest in branched colloidal gold nanosystems has gained increased traction due to the structures' outstanding optical and plasmonic properties, resulting in utilization in techniques such as surface-enhanced spectroscopy and bioimaging, as well as plasmon photocatalysis and photothermal therapy. The unique morphologies of nanostars, multipods, urchins, and other highly branched nanomaterials exhibit selective optical and crystallographic features accessible by alterations in the respective wet-chemical syntheses, opening a vast array of useful applications. Examination of discriminatory reaction conditions, such as seeded growth (*e.g.*, single-crystalline *vs.* multiply twinned seeds), underpotential deposition of Ag(I), galvanic replacement, and the dual use of competing reducing and capping agents, is shown to reveal conditions necessary for the genesis of assorted branched nanoscale gold frameworks. By observing diverse approaches, including template-directed, microwave-mediated, and aggregation-based methods, among others, a schema of synthetic pathways can be constructed to provide a guiding roadmap for obtaining the full range of desired branched gold nanocrystals. This review presents a comprehensive summary of such advances and these nuances of the underlying procedures, as well as offering mechanistic insights into the directed nanoscale growth. We conclude the review by discussing various applications for these fascinating nanomaterials, particularly surface-enhanced Raman spectroscopy, photothermal and photodynamic therapy, catalysis, drug delivery, and biosensing.

1. Introduction

1.1 Introduction of branched gold nanoparticles

Since Michael Faraday's famous 1857 lecture entitled "Experimental Relations of Gold (and other Metals) to Light" the world at large, from scientists to artists, has been fascinated by the

Department of Chemistry, University of Missouri-Columbia, Columbia, MO 65211, USA. E-mail: bakergar@missouri.edu

Asher Siegel is pursuing his Ph.D. in Chemistry at the University of Missouri-Columbia under the supervision of Professor Gary Baker. He earned his B.A. degree in Chemistry from Skidmore College in Saratoga Springs, New York in 2016. His current research focuses on synthesizing aniso-tropic noble metal nano-particles—with particular emphasis on photochemically controlled and plasmon-mediated methods—for use in energy, biomedical, and sensory applications (e.g., SERS, catalysis, and photothermal therapy).

Gary Baker received his Ph.D. in 2001 from the University at Buffalo under the direction of Frank Bright. He was a Frederick Reines Postdoctoral Fellow at Los Alamos National Laboratory before transitioning in 2005 to Oak Ridge National Laboratory as a Eugene P. Wigner Fellow and research scientist. In 2011, he relocated to the University of Missouri where he is Associate Professor in the Department of Chemistry. He currently leads a research group focused on two primary areas: (i) ionic liquids and deep eutectic solvents designed for diverse tasks and (ii) the growth of bespoke nanoparticles exhibiting features tailored to theranostics, photoacoustic bio-imaging, and catalysis.

relationship between colloidal metals and optical properties.[1,2] Perhaps due to the inherent human interest in precious metals that can be tracked for millennia, this enchantment has resulted, in part, in the field of nanoscience. For current day researchers the ever-increasing interest in the field of nonbulk materials may be driven by a desire to constantly push the boundaries of control to the atomic level and beyond.

As gold-based nanoparticles (AuNPs) continue to amass attention due to their application in a broad range of scientific fields, it becomes necessary for those researching the development of such materials to fully realize their potential. To this end, an understanding of the techniques used to precisely tune the morphologies of noble metal nanomaterials is of vital importance. Through the years the synthesis of a great number of gold nanomaterial morphologies has been realized through careful experimental considerations including spherical nanoparticles,[3] nanorods (AuNRs),[4] nanoprisms,[5] nanocubes and cages,[6] and an assortment of concave[7] and hollow[8] nanomaterials, as well as the focus of this review, branching morphologies.[9]

The interest in branching AuNPs largely derives from the exhibition of their enhanced optical and catalytic properties, as well as synthetic methods that demonstrate "greener" and less toxic reagents than other anisotropic gold nanomaterials.[10] Branching particles have also demonstrated assembly-based plasmonic properties; coupling of plasmon modes can occur if the particles are separated by a small enough distance, expanding the possibilities of application.[11] The introduction of thorns, branches, spikes, and petals into a field mostly led by ordered and symmetrical morphologies provides inroads for efficiency in various applications that have yet to be realized. As such it is worthwhile to define the parameters that dictate the resulting nanostructures to help provide an experimental roadmap towards the specific tuning of these materials.

1.2 Scope of review

In this review article we describe common methodologies towards the synthesis of branching AuNPs such as gold nanostars (AuNSs),[12–14] nanoflowers (AuNFs),[15–17] nanourchins (AuNUs),[18–20] nanodendrites (AuNDs),[21–23] multipods,[24–26] and a variety of miscellaneous shapes such as snowflakes[27,28] and nanoarrows.[29,30] In particular, this article focuses on the common synthetic techniques utilized by researchers to achieve greater shape and size control over these nanomaterials through considerations such as shape-directing agents, solvent, and reactor conditions. Finally, common uses of branching AuNPs have been described with a specific description of the nanomaterial parameters necessitated by each application that are tuneable through procedural choices.

2. Precursor methodology considerations

While a scrutinizing eye must be used in selecting from the large variety of synthetic parameters, experimental methods, and reaction vessels, the most fundamental choice that must be

made when seeking to design branching AuNPs is that of a seeded or seedless growth method. It is even reasonable to categorize all syntheses of these materials into either seeded or seedless growth as the choice is so pivotal to the resulting morphology.[31] The advantages and disadvantages of each method have been described as well as the underlying considerations that must be made with each synthetic route.

2.1 Seeded growth

The role of seed precursors demands more scrutiny than many other procedural choices in the synthesis of these nanosystems. The choice of seed-mediation allows for the temporal separation of nucleation and growth processes, leading to better control over the shape and size of the resulting nanosystems.[32,33] In seed-mediated growth of gold nanosystems, a typical reaction witnesses small, spherical gold nanoparticles acting as nucleation centres for the preferential deposition of additional Au(0) atoms. By adjusting parameters such as temperature and pH of the solution as well as the injected Au(III) : seed ratio, spherical citrate-stabilized gold nanoparticles can be grown to sizes exceeding 200 nm.[34] In the growth of branching gold nanosystems, isotropic growth can be stunted by interactions between surfactants or ions with specific crystal faces, driving selective deposition of free gold onto unblocked surfaces. The roles of such shape-directing agents will be discussed in later sections; here instead the choice of seed crystallinity, size, and relative concentration will be described.

Accordingly, the crystalline structure of the precursor seed plays a crucial role in the final morphology of the nanosystem. Wulff's theorem states that a singular fcc metal crystal, like Au, would form a truncated octahedron if formed under inert conditions. When formed in solution however, the crystals may assemble into alternate structures due to differences in facet surface energies attributed to interactions with capping agents and the solvent itself. Crystal structures that do follow the Wulff construction in solution include Au single crystalline seeds, consisting of a mix of low index [111] and [100] facets. As with most seed-mediated syntheses the growth process can be controlled by selective adsorption of ions and capping agents. However, some researchers have proposed that single or multiply twinned seeds are necessary to facilitate the growth of branches in noble metal particles.[35,36]

Under this assumption, the pathway for single crystalline seed-grown branching nanoparticles comes from the development of twin defects through a coalescence/fusion mechanism.[37] As facet-selective deposition occurs onto the gold seeds and size begins to increase, structural fluctuations in the single crystalline species are observed; in order to lower the overall energy of the enlarged particle, the twinning motif can change, inducing growth of additional twin planes and resulting in a seed morphology more suitable for branched particle growth (Fig. 1).

This process of single crystalline seed evolution was recently investigated in detail through the synthesis of multi- and six-branched gold nanostars by Atta *et al.*[38] A typical creation of
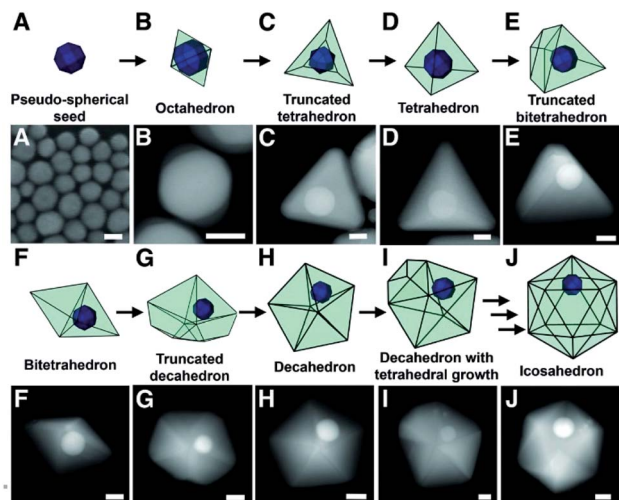
Fig. 1 Models and STEM images depicting the proposed growth pathway of a single-crystalline seed in a plasmon-mediated reaction, taken at various points in the same reaction. (A) STEM image of the pseudo-spherical single-crystalline Au seeds. (B to J) STEM images of bimetallic particles with (B) octahedral, (C) truncated tetrahedral, (D) tetrahedral, (E) truncated bitetrahedral, (F) bitetrahedral, (G) truncated decahedral, (H) decahedral, (I) decahedral with an additional tetrahedral growth, and (J) icosahedral morphologies. Scale bars, 25 nm; reprinted with permission from ref. 37. Copyright © 2012 American Association for the Advancement of Science.
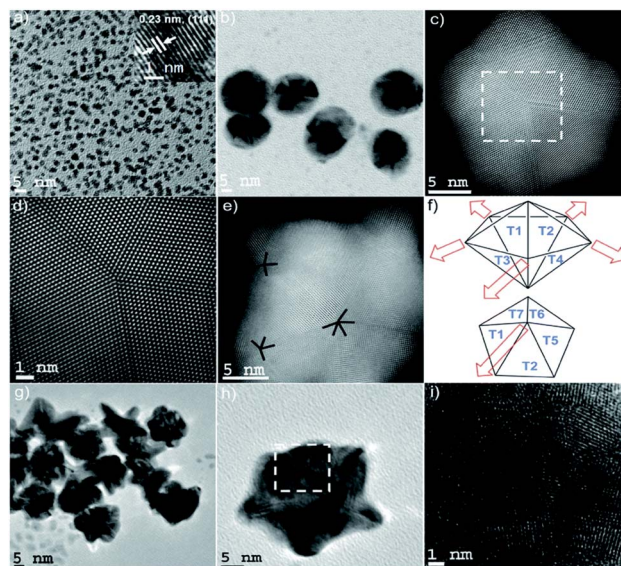

Fig. 2 (a) TEM micrograph of the seeds with an average diameter of 3 nm. The HRTEM micrograph (inset) shows the single crystalline morphology of the seed, with an interplanar spacing characteristic of the {111} plane in FCC gold. (b and c) TEM and STEM micrographs of penta-twinned intermediate seeds isolated within the first instance of growth of the 6-branched stars. (d) High resolution STEM image of the selected area of (c) exhibiting a fivefold symmetry. (e) STEM image of a typical penta-twinned intermediate seed showing one five-fold symmetry and two four-fold symmetry defects, which correlates with the 3D construction of the decahedral morphology of the penta-twinned intermediate seeds. (f) Representation of spike growth from decahedral seeds. Top image: Schematic side view identifying the spike growth directions on seeds such as that shown in (e). Bottom image: Schematic top view representing five neighbouring facets. (g–i) TEM and HRTEM images of multiply twinned intermediate seeds isolated within the first instance of growth of the multibranched stars. Reprinted from ref. 38 with permission from the Royal Society of Chemistry.

the AuNSs in question consisted of the synthesis of single crystalline seeds with (111) planes by reduction of HAuCl$_4$ by NaBH$_4$ in the presence of surface Triton X-100 at various concentrations. The seeds, AgNO$_3$, and ascorbic acid were added to a growth solution of HAuCl$_4$ in Triton X-100, the concentration of which was equal to that of the seed solution. By arresting the nanoparticle growth with n-pentane thiol at 10 s after reagent addition to the growth solution, the evolution of the seeds could be observed (Fig. 2).

At high ascorbic acid concentrations, the seeds develop into multiply twinned intermediates, resulting in multi-branched AuNSs. The excess reducing agent is believed to cause the migration of gold atoms to low energy facets such as {111} by increasing the negative charge on the seeds. Conversely, at lower ascorbic acid concentrations, a slower reduction of Au(III) takes place, resulting in penta-twinned intermediates appropriate for the growth of the six-branched AuNSs. These results strongly suggest that while crystalline defects may be necessary for such branching anisotropic growth, such twinning can be both induced and specifically tuned by altering the reactant.

The number of surface defects in polycrystalline seeds however depends on their size.[39,40] A recent publication by Indrasekara et al. on the synthesis of surfactant- and capping-agent-free AuNSs can serve as a model system to study the effect of seed size on the resulting morphologies as it eliminates the influence additional shape directing-agents may have on pre-branch-growth.[41]

The researchers synthesized 5 nm and 12 nm gold nanoparticles capped by citrate, through modified Turkevich methods. The chosen seeds were added to a gold chloride

solution under acidic conditions. 5 s after the seed addition, a small aliquot of AgNO$_3$ was injected followed by, 5 s later, AA. The AuNSs synthesized with the smaller seeds yielded smaller core and tip-to-tip diameters than those with the 12 nm seed. Meanwhile the branches resulting from the 5 nm seeds are relatively longer, but no differences in the number of branches were observed despite the assumed increase in defects in the 12 nm seeds (Table 1).

A more dramatically significant parameter to consider in seeded-growth structures is the ratio of seeds to Au(III) (R_{seed}). In the same work by Indrasekara et al. an increase in this ratio, regardless of seed size, resulted in a branch length : core size decrease, core size decrease, and a branch density decrease. As the number of seeds increases relative to the free Au(III) ions the amount of free-gold that can be deposited onto each seed decreases, understandably limiting growth. Consequently, at lower R_{seed} values, the abundance of Au(III) leads to increased branch density and overall length, resulting in a red-shifting of the main LSPR mode. An increased number of branches and length inevitably leads to more dispersity in the branch morphologies themselves, causing broadening of the LSPR band (Fig. 3).

Table 1 Dimensions of the features of AuNSs and their LSPR peak positions as determined by TEM analysis; adapted with permission from ref. 41. Copyright © 2018 American Chemical Society
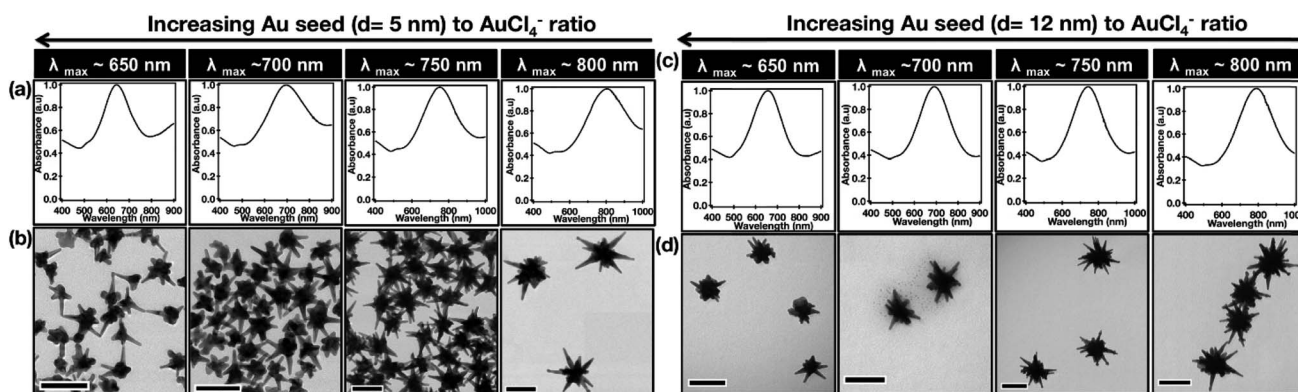
AuCl$_4^-$/mol	Ag$^+$/mol	Quantity of seeds/particles	LSPR$_{max}$ (nm)	Core diameter (nm)	Tip–tip distance (nm)	Branch density
Change in the amount of $d = 5$ nm Au seeds in growth solution						
2.5×10^{-6}	1.02×10^{-7}	2.5×10^{11}	800	93 ± 11	145 ± 30	~7–8
2.5×10^{-6}	1.02×10^{-7}	5.0×10^{11}	738	70 ± 9	105 ± 28	~8–10
2.5×10^{-6}	1.02×10^{-7}	1.0×10^{12}	690	57 ± 8	80 ± 16	~5–6
2.5×10^{-6}	1.02×10^{-7}	2.0×10^{12}	658	46 ± 7	67 ± 15	~5–6
2.5×10^{-6}	1.02×10^{-7}	3.0×10^{12}	638	39 ± 6	59 ± 14	~4–5
Change in the amount of $d = 12$ nm Au seeds in growth solution						
2.5×10^{-6}	1.02×10^{-7}	1.5×10^{9}	800	105 ± 13	148 ± 23	~9–10
2.5×10^{-6}	1.02×10^{-7}	3.0×10^{9}	750	89 ± 11	130 ± 18	~9–10
2.5×10^{-6}	1.02×10^{-7}	4.5×10^{9}	696	86 ± 27	114 ± 36	~6–7
2.5×10^{-6}	1.02×10^{-7}	7.5×10^{9}	650	64 ± 10	89 ± 17	~5–6
2.5×10^{-6}	1.02×10^{-7}	1.0×10^{8}	630	67 ± 17	50 ± 12	~4–5
Change the Au^{3+}/Ag$^+$ molar ratio with $d = 5$ nm Au seeds in growth solution						
2.5×10^{-6}	2.50×10^{-8}	1.0×10^{12}	658	104 ± 13	187 ± 32	~3
2.5×10^{-6}	5.10×10^{-8}	1.0×10^{12}	742	90 ± 13	134 ± 30	5–6
2.5×10^{-6}	2.04×10^{-7}	1.0×10^{12}	782	96 ± 16	137 ± 26	~10
2.5×10^{-6}	3.06×10^{-7}	1.0×10^{12}	822	68 ± 9	136 ± 31	~15

Furthermore, not only can the R_{seed} value affect the resulting branch length : core ratio, but also the magnitude of the morphological evolution of the particles during the growth process. As many branched nanoparticles are formed an inherent blue-shift in the LSPR can be observed as gold atoms located on high energy facets migrate in an effort to lower the overall particle surface energy.[42] In the synthesis of seed-mediated gold nanostars utilizing hydroquinone as both a capping and a reducing agent it was discovered that such a blue-shift during particle evolution could be minimized relatively by lowering the relative seed concentration.[43] The lower seed population may allow for more complete surface adsorption by the hydroquinone, arresting further possible evolution.[44]

This facile method for morphological and size control of branched nanoparticles was demonstrated by the Vo-Dinh group in their seed-based, silver-mediated synthesis of gold nanostars for *in vivo* tumor imaging.[45] By simply adjusting the precursor seed concentration at constant AgNO$_3$, ascorbic acid, and HAuCl$_4$ concentrations the group demonstrated synthesis of highly monodisperse gold nanostars at sizes of 30 or 60 nm. The researchers examined the tumor accumulation rates of these nanoparticles and observed both a higher presence and deeper tissue penetration of the 30 nm AuNSs when compared to their 60 nm counterparts. This simple synthetic adjustment allows for significant changes to particle morphology without modification or addition of reactants that may increase biocompatibility or cytotoxicity of the nanomaterials.

As seed-mediated growth reactions are not one-pot, the systematic order of seed addition to the synthesis must be considered as well. Barbosa *et al.* identified that the addition of

Fig. 3 Comparison of the optical absorbance features and morphological characteristics of AuNSs with similar main LSPR peak positions (λ_1) obtained by using Au seeds of different sizes. Normalized absorbance spectra (a and c) and the TEM micrographs (b and d) of AuNSs synthesized using varying amounts of (a) $d = 5$ nm and (b) $d = 12$ nm Au seeds with λ1 max at 650, 700, 750, and 800 nm. Scale bar 100 nm; reprinted with permission from ref. 41. Copyright © 2018 American Chemical Society.

Table 2 Qualitative comparison of the seed-mediated *versus* seed-less synthesis methods of branching gold nanoparticles

Seed-based syntheses	Seed-less syntheses
Defined growth template from precursor seeds	A more sensitive nucleation phase
Greater control over particle size and morphology	Lesser control over particle size and morphology
Relatively insensitive to reaction condition changes	Highly sensitive to reaction condition changes
Not one-pot reactions	One-pot reaction
Often must utilize harsh reagents	Can easily rely on "green" reagents

the seed precursor to the growth solution prior to full Au(III)–Au(I) reduction resulted in higher polydispersity of the resulting branching products due to oxidation of the seeds themselves.[46] Conversely, if the addition of the seeds to the growth solution is delayed, nucleation of the Au salt can be observed.[47] Identifying optimal time-of-addition conditions can be accomplished by observing the reduction of Au(III) to Au(I) by monitoring the UV-Vis extinction spectrum of the growth solution; the reduction of Au(III) witnesses the diminishment of the characteristic 314 nm absorption.

While the morphology-directing influence of surfactants and ions such as Ag(I) and halides cannot be ignored in seed-based syntheses of branching AuNPs, the selection of the appropriate gold nanoparticle precursor plays a significant role and must be approached with extreme scrutiny. While this review has focused on isotropic gold nanoparticles, as they are the system most often used for seeded growth, the utilization of anisotropic gold seeds is described periodically in later sections.
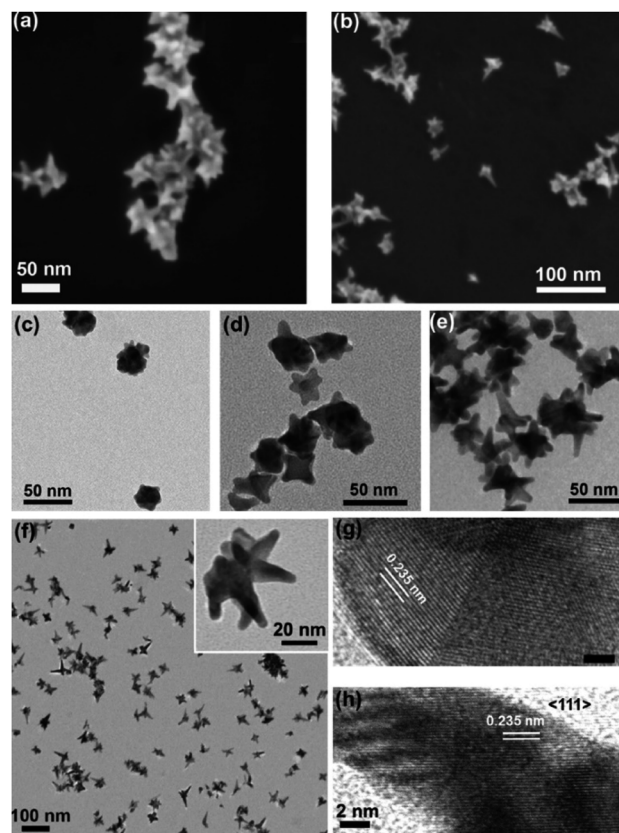
2.2 Seedless growth

The use of a gold seed precursor does offer some additional controllability in the final morphology of branching gold nanosystems based on seed size and crystalline structure (Table 2). However, due to minor heterogeneities in the structures of the seeds, this method of synthesis often leads to polydispersity in both size and shape of the resulting morphologies.[48–50] Alternatively, the one-pot, seedless method is primarily dependent on the choice of reducing agent and surfactant. Significant drawbacks do exist as such shape-directing agents (*e.g.* PVP and CTAB) strongly adsorb onto the gold surface, limiting application without additional "clean up" of the samples.[51]

It is of great interest then in a seedless approach to consider more mild, water soluble, and biocompatible reducing/capping agents to limit such barriers in the utilization of the nanosystems in SERS, biolabeling and therapeutics.

A recent example of seedless-mediated AuNFs synthesized under these considerations was demonstrated by Kariuki *et al.*[52] Using a poly(pyromellitic dianhydride-*p*-phenylenediamine) (PPDD) water soluble polymer as both a reducing and a capping agent, the polycrystalline flowers demonstrated well-resolved peaks of (111), (200), (220), and (311) with preferential growth in the ⟨111⟩ direction, a deposition pattern in line with the face centred-cubic structure of Au. Upon varying the polymer concentration it is likely that the rate of reduction of the free gold ions increased, causing rapid deposition onto the preferred facets. As such, the LSPR peak of the AuNFs was able

to be selectively red-shifted to ∼750 nm making these flower-like structures ideal candidates for imaging techniques such as surface enhanced Raman scattering (SERS).

The ability to control the morphology within seedless syntheses is paramount to their viability in application. While the tunability of seed-based syntheses of branching AuNPs is highly dependent on the R_{seed} value, Webb *et al.* demonstrated the tunability of seedless 4-(2-hydroxyethyl)-1-piperazineethanesulfonic acid (HEPES)-reduced

Fig. 4 Scanning electron microscopy images of AuNSs synthesized by (a) 160 mM HEPES buffer and (b) 300 mM HEPES buffer showing the three-dimensional morphology of the MGNs. Transmission electron microscopy (TEM) images of AuNSs synthesized with varying HEPES concentrations: (c) 30, (d) 100, (e) 160, and (f) 300 mM. High-resolution TEM images of AuNSs with d-spacing indicating (g) the {111} facet in the AuNS core and crystal plane twinning and (h) growth along the ⟨111⟩ direction for the AuNS protrusion. The scale bar is 2 nm in both (g) and (h); reprinted with permission from ref. 48. Copyright © 2014 American Chemical Society.

multibranched gold nanoantennas by modifying the concentrations of the two reactants, HAuCl$_4$ and HEPES, as well as the pH of the buffer (Fig. 4).[48] As the HEPES : Au(III) ratio increased (R_{HEPES}) at a constant buffer pH of 7.4 from 1.5 to 18, the resulting branches, protruding from the ⟨111⟩ direction, increased in length and thickness. As HEPES concentration increases, the additional shape-directing ligands during the nucleation phase help shape the seeds *in situ*. The weakened adsorption of HEPES molecules onto the (111) plane allows selective deposition of reduced gold atoms and growth in that direction. This level of nucleation control may not be possible if using prepared seeds as precursors.

Many of the disadvantages of a non-seeded approach can be overcome by carefully tuning the synthetic parameters previously mentioned (*e.g.* pH, reductant concentration/strength). One prominent remaining hurdle is matching the size-control demonstrated by seed-mediation. In an effort to do so, seedless silver- and ascorbic acid (AA)-synthesized AuNSs were created by carefully examining and altering the order of reactant addition of the original seed-based method by Yuan *et al.*[53,54] The seeded method procedure saw simultaneous addition of the reducing agent, AA, and shape directing agent, AgNO$_3$, added to a solution containing colloidal seeds and HAuCl$_4$. In the recent seedless method, Phiri *et al.* injected HAuCl$_4$ into a solution of AA at a low pH ($R_{AA} = 2$). After approximately 10 s of mixing AgNO$_3$ was rapidly injected, leading to AuNS formation directed through the underpotential deposition (UPD) of silver. The 10 s of mixing time before Ag(I) addition allowed for creation of necessary nucleation sites by a seed-mediated method. By adjusting the induction time allowed for the ascorbic acid and HAuCl$_4$ before Ag(I) injection, Phiri *et al.* demonstrated non-seeded growth of AuNSs comparable in terms of size control to that of the seeded-growth method. This type of procedural discrimination demonstrates the necessity for careful understanding of the experimental parameters chosen during seedless synthesis of branching AuNPs, careful control over the nucleation in particular. While seeded methods hold the advantage as the nucleation phase occurs on a template of known facet composition and crystallinity, one much consider the initial reduction of Au(III) to Au(I) as a step of heightened importance.

3. Synthetic techniques

3.1 Silver-mediated growth

The role of Ag(I) in the synthesis of anisotropic gold nanostructures has been investigated since Chang *et al.* showed that the aspect ratio of gold nanorods could be controlled by introducing AgNO$_3$ into the growth solution.[55,56] While the exact mechanism of Ag(I) is debated, the addition of silver nitrate to seed-mediated synthesis of branching gold nanoparticles allows for control over spike length, even in the absence of surfactants or templates.[35,57,58] Initial investigations into Ag(I)-mediated anisotropic growth suggested that a complexation between the Ag(I) and the commonly used capping agent cetyltrimethylammonium bromide (CTAB) resulted in the blocking of growth on specific seed faces.[59,60] Alternatively, it has been

proposed that an underpotential deposition (UPD) of up to a monolayer of Ag(0) occurs on selective facets, stopping further deposition or migration by gold ions.[61,62] While there is experimental and theoretical support for the two proposed silver-mediated methods, in both cases the presence of AgNO$_3$ appears to induce symmetry breaking at nucleation sites of single crystalline gold seeds, leading to anisotropic growth.[63] The relative ratio of Ag(I) : Au(III) determines at which point of seed growth the defects will form.

As such, the two greatest parameters to consider when preforming a Ag(I)-mediated synthesis of seeded branching gold nanosystems are the concentration of Ag(I) and the crystalline structure of the seed. Branching gold nanoparticles show distinct twin boundaries that match those of the seeds they are grown from; however, at appropriate AgNO$_3$ concentrations additional defects can be introduced.[36,62] During growth, the shape and size of branches can be subsequently controlled by increasing the concentration of AgNO$_3$ added. Atta *et al.* recently showed that the role of AgNO$_3$ in the synthesis of 6-branched stars can move beyond morphological selectivity and into tunability.[38] As the Ag(I) concentration was increased in the synthesis of the TritonX-100-capped six-branched species, branch length increased as well (Fig. 5).

The spike growth was more drastic with relatively higher silver concentration additions (8 nm per 10 μM addition from 30 to 60 μM as opposed to 2–3 nm per 10 μM addition from 60 to 100 μM). Not only did the stars exhibit branch elongation, but the branch sharpness (spike core width : tip width) increased as well. At low AgNO$_3$ concentrations, the stars will undergo surface energy minimization by relocating atoms from the high energy {111} facets on the sides of the tips to the low energy core facets. However, reports have shown that as the amount of
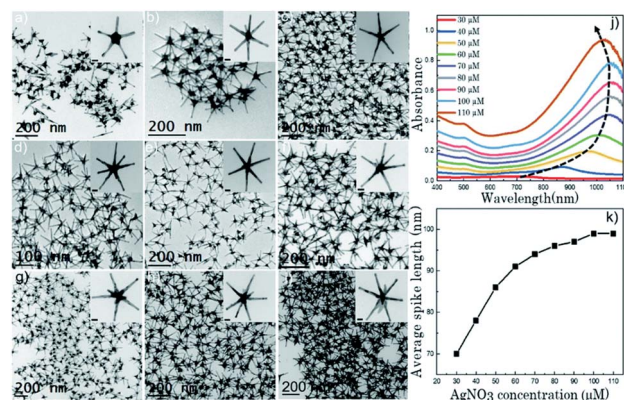

Fig. 5 (a–i) TEM micrographs of nanostars formed at different AgNO$_3$ concentrations: 30 μM (a), 40 μM (b), 50 μM (c), 60 μM (d), 70 μM (e), 80 μM (f), 90 μM (g), 100 μM (h), and 110 μM (i). The concentration of the other two chemical variables (ascorbic acid and Triton-X) was 1.6 mM and 0.15 M, respectively. Scale bars are 20 nm (inset). (j) UV-vis spectra (normalized) for each of the colloidal dispersions showing a gradual red shift with increasing AgNO$_3$ concentration as the spike length is increased, and a blue shift after 100 μM AgNO$_3$ as silver is deposited at the core. (k) Evolution of the average spike length as a function of AgNO$_3$ concentration. Reprinted from ref. 38 with permission from The Royal Society of Chemistry.

AgNO$_3$ increases, reformation decreases and the spikes maintain their sharpness; deposition of a monolayer or sub-monolayer of Ag atoms helps to stabilize the gold atoms through Au–Ag–Cl interactions.[37,64] Exploitation of this mechanism may allow for control over branch length that exceeds that of nearly all the other common synthetic parameters.

The Mirkin group has been instrumental in determining the facet-selectivity of Ag(I) ions in such syntheses. Such a study by Personick et al. demonstrated the synthesis of a variety of gold nanomorphologies mediated by AgNO$_3$ at different Ag(I) : Au(III) ratios.[64] CTAC-capped 7 nm gold seeds were added to growth solutions containing HAuCl$_4$, and variable amounts of AgNO$_3$, HCl, AA, and CTAC. Four different Ag(I) : Au(III) ratios led to four different morphologies: octahedral (1 : 500), rhombic dodeca-hedra (1 : 50), truncated ditetragonal prisms (1 : 12.5), and concave cubes (1 : 5). The octahedral morphologies are bound by eight {111} facets which, as the most thermodynamically favourable of the gold fcc facets, are formed in the absence of a significant amount of Ag(I) ions for direct growth. Low concentrations of silver ions are unable to completely cover large, high energy facets, leading to displacement by Au ions and Ag migration to lower energy facets where complete coverage is possible. A higher concentration of Ag(I) will successfully deposit onto and fully cover open facets and avoid displacement, driving Au deposition and growth onto lower energy facets. Through careful control of the AgNO$_3$ concentration in the synthesis, the growth phase of the nanoparticle synthesis can be carefully controlled.

This was additionally demonstrated by the Fabris group, who in a seed-based nanostar synthesis demonstrated the tuning of the particles' SPR into the shortwave infrared (SWIR) range.[65] In a selective reduction of free Au(III) ions onto the precursor surface by ascorbic acid, facilitated by TritonX-100, the researchers demonstrate a range of the nanostars' primary resonance peak from 600 to 2000 nm. This extreme, controlled SPR red-shift is attributed to an increased concentration of AgNO$_3$ in the reaction mixture. The resulting monolayer of Ag is hypothesized to increase the morphological stability of the particles, in particular of the branch tips. It is thus suggested by this author that the increased silver concentration contributes to a full silver monolayer rather than a submonolayer as proposed at times in the literature, disallowing migration of gold atoms from the peaks to low-energy core facets. The hyper-stability of the tips leads to increased branch length and the resulting SWIR extinction.

However, a disadvantage to the use of silver in such synthesis does exist. As the UPD of Ag is most efficient under acidic conditions, attempts to manipulate the growth process through increases in the solution pH may be likely to cause a loss of tunability. As such some limitations will exist if attempting to alter the reduction or capping ability of certain reagents.

3.2 Reducing agent choice

In the selective reduction of Au(III) salts in the synthesis of nanoparticles, the choice of reducing agent is significant in determining the isotropic or anisotropic morphology. Extensive

studies have examined the oxidation potential of aqueous HAuCl$_4$, with recent work from Ayeni et al. proving through cyclic voltammetry that, regardless of concentration, gold(III) chloride solutions have oxidation potentials of 0.55 V and reduction potentials of 1.23 V.[66] As such, appropriate reducing agents can be selected in order to reduce Au(III) salts to zero-valent multi-atom Au species. Moreover, the reducing agent must be of significant strength to guarantee that the reduction is an irreversible reaction. While the surface migration of gold atoms towards low energy facets and the use of etchants to remove deposited gold are both common causes of nanoparticle reshaping, instability due to reducing agent weakness may lead to full degradation of the particle. Amongst previous literature reports that does so, a recent, significant study by Rodrigues et al. describes in great detail the use of reductants on colloidal metal nanosystems and their underlying mechanisms.[67] Accordingly, this section will briefly describe common reducing agents used specifically for branched AuNPs and the influencing parameters.

Among the most common reductants in the synthesis of noble metal nanoparticles are hydrides, phenols, organic acids, and nitrogen-containing compounds. As the final morphology of the nanosystems is, at the very least, dependent on the initial reduction rate of the metal salt, the choice of reductant strength is vitally important.[42] Extremely strong reducing agents such as sodium borohydride are rarely utilized in the synthesis of anisotropic nanoparticles, as the extremely fast reduction instead often yields small, isotropic particles.[68,69] In seeded growth, such strong reductants will cause the reduction of free Au(III) ions into new spherical particles rather than deposition onto pre-existing seeds.

Alternatively, phenols such as ethylene glycol and hydro-quinone are strong enough reducing agents to reduce Au(III) in the formation of gold nanomaterials, but are susceptible to oxidation to products capable of mild reduction, making branching morphologies possible. Lee et al. showed that branched AuNPs could be synthesized using o- and p-hydrox-yphenols without additional surfactants.[70] The self-conversion of the hydroxyphenols into pyrocatechol (quinone) allowed for initial electron donation and the propagation of gold seeds. The quinone species are less reactive than their hydroxyphenol predecessors and the mild reduction helps drive secondary Au(III) reduction to Au(I), allowing deposition onto the seeds' low energy facets, forming branches. Dopamine, an amine functionalized dihydroxylphenol, used extensively in the formation of branching AuNPs, can generate secondary spikes protruding from the primary branches.[71,72] The terminal primary amine group introduces a tertiary reducing agent, leading to these thorns. Liu et al. found that at high concentrations of polyphenols such as pyrogallic acid, hydroxyl groups are oxidized into carbonyl groups. Competition between phenolic hydroxyl and carbonyl groups increases anisotropic growth protection and can result in AuNFs.[73] Phenolic synthesis of branching AuNPs suggests that such anisotropic morphology is dependent on competing and complementary reducing forces; however, the use of other mild reducing agents in the presence of other shape directing agents is widespread as well.
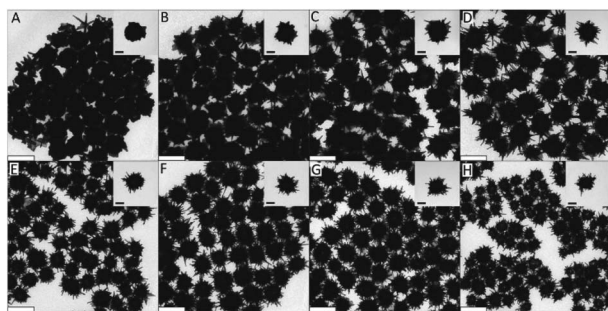
Fig. 6 (A–H) TEM images showing the morphology and branching evolution of AuNPs formed in the presence of (A) 0.77, (B) 0.92, (C) 1.07, (D) 1.34, (E) 1.97, (F) 2.63, (G) 3.49, and (H) 4.68×10^{-3} M ascorbic acid while keeping the concentrations of TX-100, HAuCl$_4$, and AgNO$_3$ under standard conditions. Scale bars are 200 nm (main) and 70 nm (inset). Reprinted with permission from ref. 78. Copyright © 2015 Wiley.

Organic acids such as ascorbic, citric, and formic acid are widely used in tandem with surfactants to achieve anisotropic gold nanoparticles. The pH sensitivity of organic acids' redox potentials allows for their use in seeded growth syntheses. Arguably the most utilized reducing agent for branching AuNPs, AA has been applied to form gold multipods,[36] stars,[74] urchins,[19] dendrites,[75] and more[26,76,77] and can be examined as a model for organic acid reductants. Work from our group has shown the facile room-temperature non-seeded synthesis of quasi-spherical gold particles by ascorbic acid as the sole reducing and capping agent.[69] However, by controlling the redox potential of AA through a pH decrease, the reducing agent is only able to reduce free Au(III) ions to Au(I) in the absence of seed catalysts. This allows for directed deposition of Au(I) atoms onto the gold seeds as directed by additional capping ligands or ions such as Ag(I) or halides. The effect of ascorbic acid in these syntheses is highly dependent on the surfactant and/or co-reductant used. Increased AA concentration in the synthesis of TritonX-100 capped burr-like AuNPs increases branch length and is attributed to increased reduction ability while CTAB-based syntheses show an inverse relationship between ascorbic acid and branch length/density (Fig. 6).[78]

Small-branching trisoctahedral gold nanocrystals were achieved by Wu *et al.* by a synthesis that demonstrated significant morphological control by adjusting the amount of AA in a seeded CTAC-capped synthesis.[79] Changes in reductant in the growth solution demonstrated control over the rate of reduction of gold atoms onto the seed, resulting in control over final morphology.

Nitrogen-containing compounds are well established as both reducing agents and capping agents in the syntheses of gold nanomaterials.[67] Regardless of structure, nitrogen–gold interactions are capable of shape-directing final nanoparticle morphology, so protonation or deprotonation can play a significant role.[80] In HEPES-based syntheses of AuNSs and gold tetrapods, the tertiary amine of the piperazine ring must be a deprotonated free radical in order to cause the reduction of gold and formation of the branched AuNPs.[48] Unlike other common reductants, amines typically reduce gold through the

donation of a singular electron resulting in radical formation.[81] The oxidized products, whether amines, imines or nitriles, are capable of coordinating with the resulting nanoparticles, and drive facet-selective growth.[67] Many biomolecules contain such nitrogen-groups and an understanding of their use as reductants is vital to the synthesis of green AuNPs.

The use of two or more reducing agents has simultaneously been employed in the creation of small, spherical nanoparticles in fundamental gold seed production, such as the Turkevich method. In these syntheses however, one strong reducing agent, NaBH$_4$, was used to reduce gold to its zero-valent state while the second, citrate, acts as a stabilizing ligand. The use of two highly effective reducing agents without a stabilizing ligand can significantly alter the mechanism for nanoparticle growth, leading to anisotropy. The reduction of HAuCl$_4$ by both tannic acid and NaBH$_4$ saw tannic acid taking on the role of a stabilizing ligand in the resulting spherical nanoparticles, as evidenced by similar results when tannic acid was replaced with the nonreducing stabilizing ligand PVP.[82] When the tannic acid-based dual reduction is undertaken with a more mild reducing agent than NaBH$_4$, ascorbic acid, the two reducing agents work in tandem, confirmed by conformational changes as the concentration of tannic acid increases, and yield both stars and urchin-like gold structures. The use of two reducing agents simultaneously can cause two-step reduction; first a nucleation event occurs directed by the more powerful reductant, followed by growth of the remaining free Au(III) ions onto the newly formed structures by the secondary reductant.

3.3 Surfactant choice

Upon reduction of a gold salt to a zero-valent species, surfactants are often needed to stabilize the colloid structures. While some reducing agents will play roles as surfactants as well, in many syntheses the choice of an additional reagent to adsorb to the nucleation growth surface will be a defining factor in the final morphology. This adsorption can change the relative growth rates of crystal facets by altering their free energies.[83]

Many surfactants will undergo adsorption on the gold crystal surface through bilayer formation.[84] As the hydrophobicity of the shape-directing agent increases, the micellar assemblies become worm-like and preferentially form elongated morphologies such as nanowires. As such head group modifications, such as ionic or zwitterionic groups, can loosen the micelle formation and help direct branching particles.

Ionic surfactants such as the frequently utilized CTAB preferentially adsorb onto the {100} crystal planes of gold seeds and are fundamental in the creation of gold nanorods by allowing for {111} planar deposition.[85] However the presence of significant twin defects in the seed precursor will weaken the binding of the surfactant and result in branch growth instead of symmetrical elongation.[86] Greater CTAB concentration per seed subsequently causes a larger number of CTAB micelles leading to increases in branch density and length as surfactant binding directs the anisotropic growth.[87]

The passivation of crystalline surfaces is better conducted by ionic surfactants than zwitterionic ones; zwitterionic

surfactants will arrange in a zigzag-type fashion to limit repulsive forces and lead to poor capping. These weakened interactions can lead to controlled anisotropic growth. Pallavicini *et al.* demonstrated such control by the zwitterionic laurylsulfobetaine (LSB) in a silver-mediated, ascorbate-reduction of HAuCl$_4$.[88] Oddly enough, LSB preferentially adsorbs onto the lower energy {111} facets, leading to Au deposition onto {220} and {002} faces. This is unusual as most ligands prefer to passivate high energy facets by adsorbing there, leaving lower energy facets open for gold deposition. This adsorption is likely due to the cationic nature of the ligand, indicating that further control over the growth of such particles can be achieved through head-group alterations.

Another class of surfactants that demands scrutiny is halide counteranions. These halides, specifically Cl$^-$, Br$^-$, and I$^-$, are known to be able to adsorb onto preferred Au crystalline facets. These effects were summarized by Kedia *et al.* as they examined the introduction of halide ions into DMF–PVP synthesized gold nanostars.[89] The addition of Cl$^-$ ions witnessed a red-shift of the LSPR peak as the spikes widened in size while the core maintained its morphology. Conversely, the addition of Br$^-$

ions resulted in an LSPR blue-shift as not only did spike length decrease but the width and the branch density as well (Fig. 7). I$^-$ ions, having the strongest affinity to adsorb onto gold surfaces among the halides, understandably had the greatest morphological effect. Instead of yielding branching particles, the synthesis produced a mixture of spherical and triangular prism-shaped particles.

3.4 Surfactant-free synthesis

The ability to synthesize and tune branching AuNPs sans surface adsorption is of great interest to many researchers. These "clean" nanosystems avoid the challenge of removing traditional capping agents such as CTAB, PVP, and DMF. However, some stability issues tend to cause drastic morphological changes in these nanosystems quite rapidly. Typically, surfactant free-synthesized branching AuNPs are coated with thiolated compounds after synthesis to delay the aging process.[90]

AuNSs were synthesized by Yuan *et al. via* a seed based (12 nm) surfactant-free method by the AA ($R_{AA} = 1.5$–2) reduction of HAuCl$_4$ in the presence of AgNO$_3$.[53] The resulting AuNSs were approximately 60 nm and demonstrated morphological control by adjusting the concentration of AA and AgNO$_3$, and pH in a similar manner to nanostars synthesized with CTAB or PVP. Poonthiyil *et al.* reported surfactant-free AuNUs through a solvent-directed synthesis at a relatively mild temperature of 60 °C.[91] HAuCl$_4$ (1 mM) was added to 50 mL of anisole solvent and allowed reaction time resulting in AuNUs (1 min) or the more thermally stable quasispherical AuNPs (15 min). Interestingly, the reaction failed to result in any gold nanostructures in the presence of thiol or amine capping agents. Finally, seedless, surfactant-less, room temperature AuNFs were obtained by a simple synthesis consisting of the reduction of 0.3 mM HAuCl4 at room temperature by 5-hydroxyindole-3-acetic acid (0.075 mM).[92] The AuNFs were shown by selected area electron diffraction (SAED) to be single crystalline with a (111) lattice plane. Not only were the nanosystems utilized for SERS and electrocatalysis, but also demonstrated fluorescent emission at 585 nm.

The adoption of these "bare" branching AuNPs is especially encouraged by the biomedical applications of surfactant-free nanosystems. By eliminating possible toxicity from common surfactants, the use of the nanoparticles as probes and sensors becomes more attractive.[92,93] Additionally, the free surface allows for conjugation of application-specific biomolecules such as immunostimulatory agents and photosensitizers.[94] Nam *et al.* synthesized surfactant-free spiked AuNPs using these very principles for the delivery of an adjuvant for immune activation of bone marrow-derived dendritic cells (BMDCs).[95] The AuNPs were synthesized through a seed-based method utilizing ascorbic acid as a reducing agent.

3.5 Galvanic replacement

Galvanic replacement is a template-driven synthesis process in which a noble metal salt such as HAuCl$_4$ encounters nanoparticles made of a metal with a lower reduction potential. In
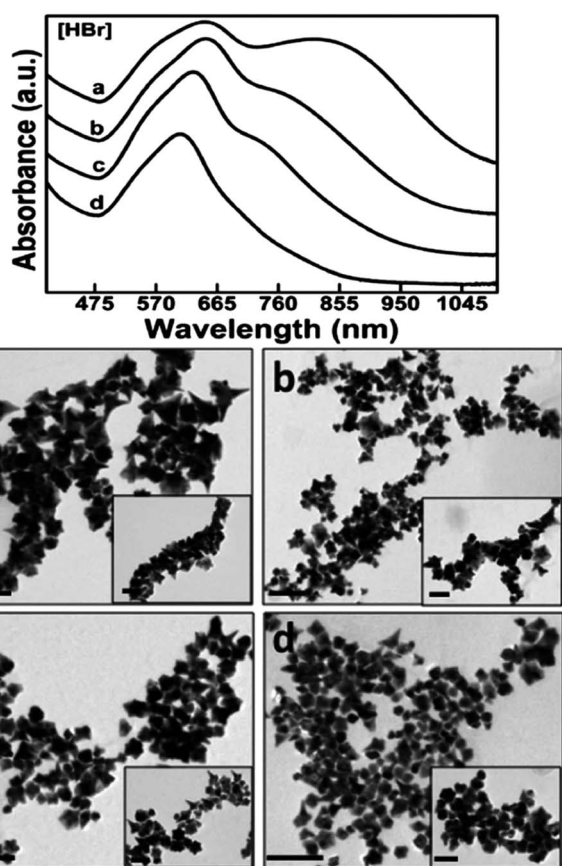

Fig. 7 The increasing addition of (a) 0.20, (b) 0.40, (c) 0.60 and (d) 0.80 mM HBr to the precursor reaction mixture clearly influences the formation as well as the self-organization of anisotropic gold nanostructures, as prominently revealed by the optical spectra and their corresponding TEM images (scale bar 200 nm with inset scale bar 100 nm). Reprinted with permission from ref. 89. Copyright © 2014 Royal Society of Chemistry.

such a case, gold will be deposited while simultaneously corroding the nanoparticle template from the inside out.[96] This process is understandably most often used for the creation of hollow nano-systems.[6,97] As a consequence of the synthetic method, many of these hollow nanostructures are considered bimetallic structures, but in some the trace amounts of the templating metal are low enough to be considered inconsequential.[98,99]

Gold flowers were produced through the galvanic replacement of resin immobilized Cu nanoparticles under surfactant-less conditions.[100] As galvanic replacement causes the reduction of Au(III) to Au(0), the deposition of which is directed (atom on top of atom) by the negatively charged resin beads, petal-like branches form from the core due to the polarization effect. Adjusting the amount of resin bound-Cu(0) used under constant (10 mM) $HAuCl_4$ concentration produces structures including nanoworms (30 mg resin immobilized Cu(0)), nanoflowers (100 mg resin immobilized Cu(0)), and nanocubes (300 mg resin immobilized Cu(0)). Copper was also used as a templating metal in the synthesis of branching gold nanoparticles in oleylamine (OAm), an organic medium.[99] The core of these branching particles had a lattice spacing of 0.28 nm, a spacing that is absent in both cubic Au or Cu but that is present in the (110) planes of the Au_3Cu alloy (Fig. 8).

The observation that there was negligible copper content in the final branching gold particles suggests that after initial alloy seed formation, the remaining copper ions were replaced through further galvanic replacement and deposition of Au(0) to the core and branches. These results suggest the further possibility of forming monometallic branching particles with lattice spacing only seen in alloy cores.

3.6 Etching

Once synthesized, it is understandably difficult to cause intentional and controlled morphological changes to branching particles. While the particles can serve as seeds for further reactions, capping ligands can be exchanged and particles further functionalized, changes to the metal framework of the

systems must be completed through oxidative etching. Just as with deposition-based growth, etching can be facet selective, allowing for greater morphological control. The reshaping of gold nanosystems through this method is dependent not only on the etching agent, but also on the surfactant and nanoparticle surface curvature.[36,101,102]

Various etchants including cyanide,[103] molecular oxygen,[104] copper ions,[105] and ferric ions[106] have been used to selectively change the morphologies of anisotropic AuNPs. An additional etching agent, hydrogen peroxide, has been used extensively over the last decade as favourable interactions with halide ions help drive the reshaping of such particles.[107,108] The effects of Cl, Br, and I ions in this process have been investigated and all found to have profound etching ability which increases along with redox potential of the ions and their Au-binding strength ($Cl^- < Br^- < I^-$).[109] It is believed that the halide ions promote gold etching by generating their diatomic species, whose favourable redox potentials provide additional oxidation channels alongside those of H_2O_2.[110] The etching of non-seeded, silver-mediated, branched AuNPs capped with CTAB by H_2O_2 in the presence of these three ions saw a continuous, time-dependent blue-shifting of the plasmon band of each nanosystem when exposed to each of the three halides, as well as a dampening in extinction intensity.

I^- expectedly showed the most dramatic effect; in fact, greater oxidation was observed in the presence of I^- at a concentration 1/10th that of the other halides. While there are often issues with controlling the size of non-seeded branched NPs, selective oxidative etching may provide a solution. The relatively lower surfactant density of the sharp arms of such nanosystems should invite easy access for oxidizing species leading to the ability to shorten branch length. Rodríguez-Lorenzo et al. demonstrated similar results in the etching of PVP-capped AuNSs by CTAB into quasispherical structures.[111] While CTAB is most often used as a stabilizing agent, the authors believe that the reshaping occurs by an Ostwald ripening process; the high binding constant of Au(I) to CTAB is attributed to a facilitated migration of gold atoms from the branch tips to the particle core. However, with this method of size control, there is a significant trade-off: loss of sharp, pronounced branch-tips, the resulting "hot spots" and their appeal in applications such as SERS.

3.7 Template-mediated growth

Of the synthetic efforts to directly control the size and shape of anisotropic particles, growth from template-mediation allows most for specific alterations. The arms of branching gold nanoparticles synthesized within mesoporous silica shell-templates can be tuned in size by altering the shell itself. The silica structures are synthesized through adaptation of the Stöber method, a surfactant-templated synthesis that allows for pore size control through surfactant choice.[112] Gold nanostars were synthesized through an overgrowth reaction by CTAB-based silica shell-coated gold seeds (Fig. 9).[113]

The addition of free Au(III) ions in the presence of a mild reducing agent, ascorbic acid, to these seeds led to branch

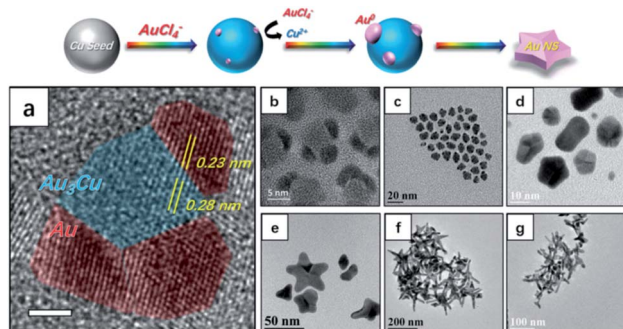**Fig. 8** Top panel illustrates the nucleation and growth of AuNSs. (a) Analysis of an HRTEM image of nucleates from panel (b). The scale bar is 2 nm. (b)–(g) TEM images of nanocrystals obtained at reaction times of (b and c) 2 min, (d) 10 min, (e) 20 min, (f) 30 min, and (g) 40 min after injection of the Au precursor. Reprinted from ref. 99 with permission from The Royal Society of Chemistry.
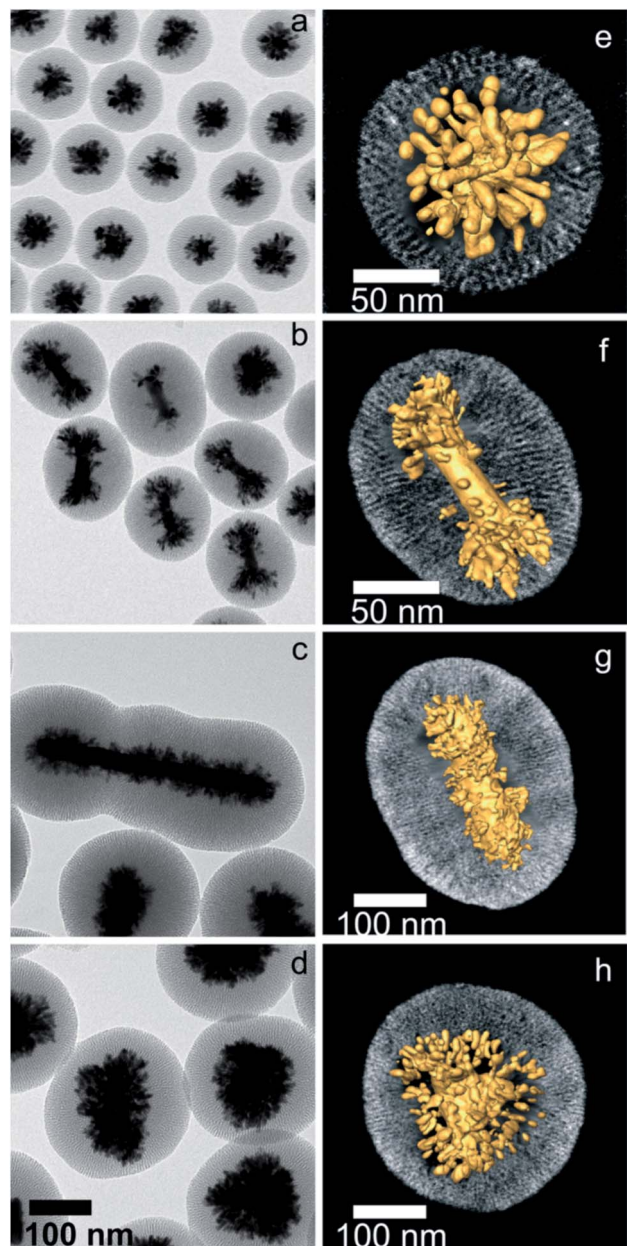
Fig. 9 2D and 3D TEM characterization of hybrid nanostructures containing different gold nanoparticles coated with mesoporous silica, after growing gold tips through the silica channels: AuNPs (a and e), single-crystal AuNRs (b and f), pentatwinned nanorods (c and g), and nanotriangles (d and h). All the images in the left panel were obtained at the same magnification. In the right panel, a visualization of the 3D reconstructions for a representative nanoparticle of each type is displayed, where the radial nature of both the channels and the gold branches can be observed. Reprinted with permission from ref. 113. Copyright © 2015 American Chemical Society.

growth along the silica pores. Upon selecting an alternate surfactant-template for the silica shells, the pore size will change, resulting in branch radius changes.

The reducing agent itself can play an additional role as a soft-template in the synthesis of branching gold nanostructures. Good's buffers have been used extensively in the synthesis of both seeded and seedless surfactant-free branching gold
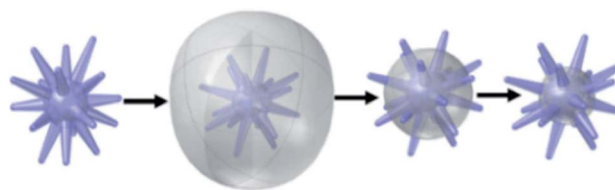
nanosystems.[114] In one such synthesis, an extreme excess of HEPES reductant both reduces Au(III) and directs the formation of the gold tetrapod morphologies.[115] The buffer self-assembles such that a bilayer of HEPES molecules forms on the gold surface, serving to direct and stabilize the branching morphology. The Odom group has demonstrated the tunability of HEPES-reduced gold nanostars; by increasing the relative concentration of the reducing agent the resulting resonance could be facilely red-shifted within the NIR region from 700 to 860 nm.[116] These stars were subsequently functionalized with a DNA aptamer (AS1411). The attachment of the aptamer onto the AuNSs increased the stability of the anticancer agents demonstrating the ability of branching AuNPs as drug delivery agents.[117]

Considering that disadvantage, a different type of etching has been utilized with branched particles, particularly with gold nanostars. Rather than causing plasmonic shifts through alterations of the metallic frameworks themselves, this alternative approach achieves LSPR tunability by coating branching AuNPs with a silica-based layer, followed by selective removal of said coating. The coating of noble metal NPs by silica has gained notable interest in recent years as a silica coating enables biocompatibility and additional surface-functionality.[112,118,119] Silica-coated gold nanostars are of particular interest for their application in SERS, singlet-oxygen generation, as photothermal agents, and more.[120,121] The silica coating is applied to already-formed gold nanostars by variations of the Stöber method, an ammonia-catalysed sol–gel reaction involving the hydrolysis of tetraethylorthosilicate (TEOS). Atta et al. performed a reverse Stöber method to successfully coat gold nanostars with a silica shell, replacing the CTAB surfactant with TEOS (Scheme 1).[122] By selectively etching away the silica shells with NaBH4, the shell was removed isotropically, allowing researchers to tune the optical properties of the nanoparticles by changing the size of the quasispherical core while keeping the tips of the branches, needed for the "lightning rod" effect, intact.

4. Nonaqueous reaction conditions

4.1 Organic solvents

While the majority of wet syntheses for branched AuNPs occur in aqueous solutions, the use of organic solvents allows for a higher maximum reaction temperature and a variety of organic shape directing agents and surfactants.[123] Additionally,

Scheme 1 Schematic illustration of the morphologies of silica coating and etching to expose only variable amounts of the spike's surface. Reprinted with permission from ref. 122. Copyright © 2020 Wiley.

© 2021 The Author(s). Published by the Royal Society of Chemistry

solvent–particle interactions will differ under organic conditions and can lead to anisotropic growth. Gold nanomaterials synthesized in alcohols without excess surfactant can lead to an asymmetric charge distribution on the particle surface.[123] While this may lead to aggregation it can also help control the rate of deposition and the targeted crystalline facets, leading to branched growth. Stanishevsky *et al.* demonstrated that the reduction of HAuCl$_4$ by AA, followed by injection of additional gold salt could be morphologically controlled by increasing the methanol content of the water/methanol solvent.[124] The additional HAuCl$_4$ added into samples of higher methanol composition yields branched particles without an additional shape-directing agent as deposition is driven onto specific facets. The Senthil Kumar group showed that DMF, a polar aprotic organic solvent, has shown the ability to produce branching AuNPs with precise morphological control in the presence of a shape-directing agent such as PVP.[124,125] The complexation of DMF and PVP facilitates a kinetically controlled growth that can be controlled by the addition of HCl. Initially formed gold seeds will compete with PVP molecules for DMF interactions, reducing the growth rate of the particles enough to lead to branched morphologies. Additional work performed by the Liz-Marzán group has shown that, while PVP is typically unable to reduce gold under ambient conditions without a photochemical influence, at high enough concentration in a DMF solvent system, PVP is able to reduce Au(III) and result in multipods.[126]

4.2 Ionic liquids and deep eutectic solvents

New classes of solvents such as ionic liquids (ILs) and deep eutectic solvents (DESs) have gained significant attention in the production of noble metal nanoparticles. As green and designer solvents, ILs demonstrate tuneable physicochemical properties that can assist in the tuning of anisotropic gold nanosystems.[127]

Qin *et al.* demonstrated the synthesis of three-branched gold nanotips in a [BMIM][PF$_6$] ionic liquid–formamide 1 : 1 solvent ratio. The kinetically controlled synthesis was tuned by altering the IL–formamide ratio, achieving monodisperse structures as the ratio decreased and a balance between diffusion rate and reaction rate was achieved. Anouti *et al.* demonstrated that the low mutual miscibility between a protic IL such as BEHAF and water led to the formation of multipod AuNPs while the same synthesis in water, DMF or a miscible IL yielded quasispherical AuNPs.[128] The authors concluded that the anisotropic growth in these particles is caused by the BEHAF preferential adsorption onto the (111) surfaces allowing for selective growth onto higher energy facets. While passivation of high energy facets to minimize surface energy is the typical mechanism, the affinity to the low energy (111) surfaces may be due to the protic nature of the IL, a preference demonstrated through recent work by Lin *et al.*[129] DESs, although closely resembling room-temperature ionic liquids, are attractive alternatives due to their low cost, nontoxicity, and biodegradability.[130] Additionally, the extensive hydrogen-bond network of DESs acts as a soft template for shape-control of noble metal nanosystems.[131,132] AuNFs were synthesized in DES for use in SERS.[133] While reduction of HAuCl$_4$ occurred at any significant DES concentration, flower-
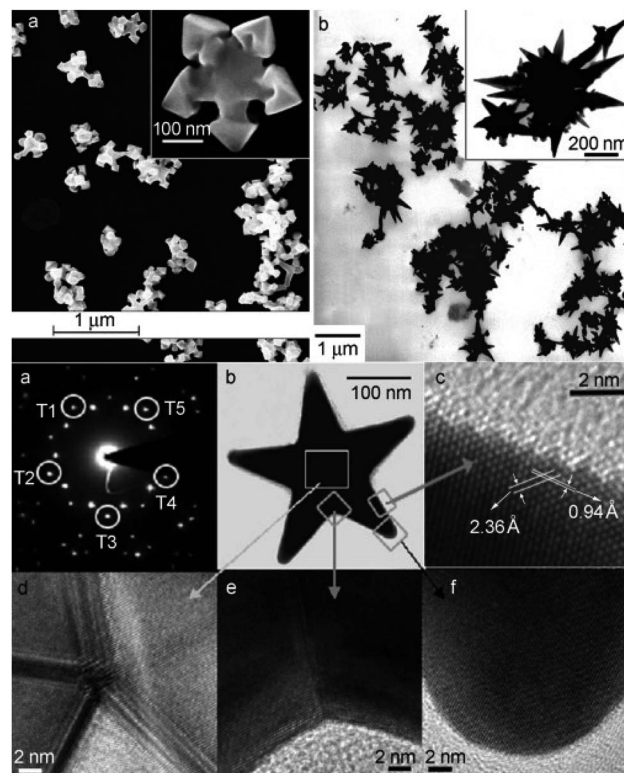

Fig. 10 Top: SEM images of the snowflake-like AuNPs (a) and TEM images of Au nanothorns (b). Bottom: HRTEM images of AuNPs recorded along [110] (b–f) and the SAED pattern (a). Reprinted with permission from ref. 132. Copyright © 2008 Wiley.

like structures occurred at higher DES percentages as the weakened protection of the growing gold structures by the solvent rather than water allowed for branch formation along the (111), (200), (311) and (222) facets. As the DES percentage increased above 10% multipod morphologies were observed instead. These morphological changes may be due to a relationship between the gold reduction rate and DES concentration; as the amount of DES increases, so does the gold deposition rate onto the branch tips, leading to the creation of energetically preferred 2D pod-like structures.

Liao *et al.* utilized DES solvents to obtain branched AuNP structures by altering the water content in the DES.[132] The absence of water caused the formation of snowflake-like AuNPs with branches along the (111) facets while increasing water content to 5000 ppm yielded AuNSs (Fig. 10). The higher water concentration is then proposed to increase the reaction rate while also disrupting the liquid templating role that the DES may be playing.

5. Reaction conditions

5.1 Microwave-assisted reactions

Typically, nanostructure syntheses that require high temperatures are performed by heating reagents by conduction and convection in an oil-bath. Microwave dielectric heating has been used less frequently but to great efficiency; MW

irradiation's reactionary advantages include homogeneous nucleation due to uniform heating, enhancement of the metallic ion reduction rate, superheating of solvents, and perhaps most importantly, selective formation of specific morphology.[134] When utilized in tandem with PVP–SDS template-mediated growth, microwave-assisted ginger-like branching gold nanoparticles were synthesized, while ordinary heating methods led to spherical nanoparticles.[135,136] The authors found that the soft-template nature of PVP–SDS should be further weakened by microwave irradiation, which, when combined with the microwave-promoted rapid and abundant synthesis of gold seeds, led to anisotropy. Ngo *et al.* have recently shown that microwave-assisted, seed-based synthesis of monodisperse gold nanostars is not only possible, but also tuneable.[137] By altering the concentration of AA, CTAB, gold seed, and AgNO$_3$, the researchers were able to take advantage of the microwave irradiation to yield rapidly formed, highly homogeneous nanostars. The use of both MW irradiation and ultrasound in the synthesis of template supported-metal nanoparticles has shown that changes in the duration, intensity, and any pulse-like flux rates of irradiation can alter the final morphology of the nanosystem.[138–140]

5.2 Microfluidic synthesis

When considering the tunability of nanosystems it is essential to promote controlled, consistent growth while limiting new nucleation events.[141] This separation can be achieved in traditional batch-reactor syntheses by temperature control or through weakening of reduction agent strength.[141,142] The use of microfluidic reactors allows for such separation while maintaining otherwise suboptimal conditions by both timely and spatially separating nucleation and growth phases within the reaction (Scheme 2).[143]

Higher surface area-to-volume ratios, mixing rate control, and readily available, accessible components make such reactors intriguing.[4,144] While synthesis of branching gold

nanosystems through fluidic reactions has not been widely investigated, spherical nanoparticles and nanorods have shown great tunability by altering flow rates of one or more reaction inputs.[145,146] Silvestri *et al.* demonstrated millifluidic synthesis of gold nanostars through a seedless, silver-mediated synthesis.[143] The final nanostar morphology was highly influenced by the flow rate; a slower flux rate caused inefficient mixing resulting in a polydisperse product while a higher flux rate yielded large nanocrystals and clusters. Another group obtained star-like gold nanosystem intermediates by adjusting the pH of the reaction through an increased flow rate of an alkaline growth solution.[145] The robustness and accessibility of the microfluidic systems, as well as easily tuned environmental parameters associated with them, make them exciting new platforms for future study.

6. Towards common morphologies

As previously mentioned, the creation of branching AuNPs is often dependent on crystalline facet-driven adsorption of free Au(III) ions onto a nucleation site. However, as protruding arms form during the growth phase the creation of additional facets as well as changes to the free energy of pre-existing facets does occur. Consequently, the number of branching AuNP morphologies is considerable.
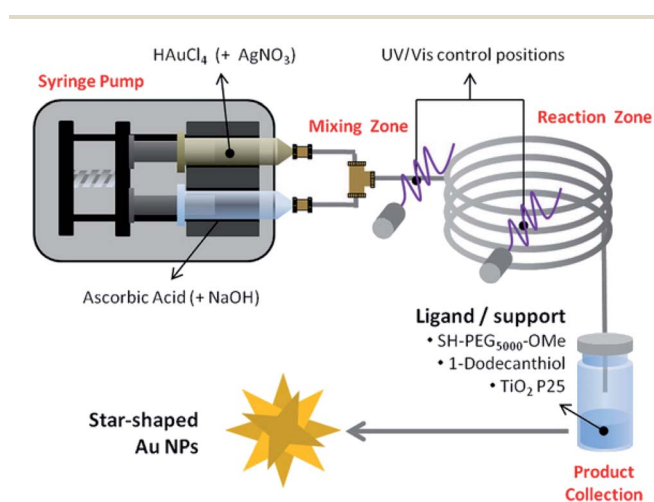
Among the most common morphologies of branching AuNPs are stars, flowers, urchins, dendrites and multipods. As there is great overlap in the applications, and at times even the synthetic methods of these nanosystems, the clearest distinction between them comes from shape.

While both nanostars and multipods can be identified by their arm-like protrusions, nanostars are traditionally defined by high numbers of narrow branches, sharp tips, and a small particle core. Multipods however contain a few broad arms with wide tips and typically smaller arm : core size ratios than their star counterparts. Nanourchins also contain sharp, narrow branches; however, the protrusions exist in far greater numbers and are significantly shorter than those seen in nanostars, much like their namesake of the sea urchin. Similarly, both nanoflowers and dendrites are appropriately named; the former can be identified by petal-like nanosheet protuberances while the latter resemble the branching extension of a nerve cell.

In the following sections the most common branched AuNP morphologies will be examined with specific emphasis on examples of tunability both during nucleation and growth phases as well as after.

6.1 Nanostars

Due to recent increased interest in the applications of noble metal nanostars towards catalysis, optical imaging, and biomedical uses, many pieces of significant review literature have explored arguably the most common branching nanoparticle morphology.[147–150] As such, this section will focus on the most common strategies for synthesis and morphological tuning of AuNSs.

Scheme 2 Schematic representation of the bench-top reactor designed for the synthesis of surface functionalized AuNSs. Reprinted with permission from ref. 143. Copyright © 2017 Wiley.

The seminal work of AuNS synthesis was conducted by a modified gold nanorod procedure involving the reduction of free Au(III) ions onto gold seed precursors by ascorbic acid in the shape-directing presence of cetrimonium bromide (CTAB).[86] Nehl *et al.* found in this work that the added presence of NaOH resulted in a kinetically controlled faster deposition of gold ions. Upon rapidly increasing the solution pH, it is likely that the chelating ability of ascorbic acid is altered as concentration of the less stable dianion increases, leading to branching anisotropic growth as the adsorption strength of the acid on the nanoparticle surface weakens at lower energy facets.[151]

By adjusting the concentration of NaOH in a seedless and template-less synthesis of gold nanostars, Kedia *et al.* were able to use pH adjustments prior to the nucleation phase to tune AuNSs (Fig. 11).[149] In this synthesis, the pH of an aqueous solution of polyvinylpyrrolidone (PVP) in *N,N*-dimethyl formamide (DMF) was adjusted through the increasing addition of NaOH prior to addition of a HAuCl₄ aqueous solution. As the pH of the DMF–PVP complex increases, the tips dull and become broader, transforming from star morphologies into multipods. It is likely that the higher NaOH concentration, which results in an increased reduction capability of the DMF–PVP complex,

induces a faster nucleation rate of the gold seeds, causing a broadening of the resulting branches.

While synthetic control over nanostar size, branch number and branch length is vital, the full potential of these nanosystems cannot be achieved without control over the morphological symmetry as well. The AuNSs obtained by Niu *et al.* through an icosahedral seed-mediated approach highlights that highly symmetrical nanostars are obtainable through careful consideration of precursor crystallinity combined with kinetic growth control through reductant concentration.[152] For example, in the stars produced by Niu *et al.*, dimethylamine (DMA) selectively adsorbs onto the {321} high-index facets of the icosahedral seeds. Relatively high concentrations of DMA combined with relatively slow growth kinetics allow for the seeds to evolve into nanostars with {321}-faceted arms. These results are consistent with a previous example of work by Kedia *et al.* who observed that a faster nucleation rate caused by a pH adjustment caused a broadening of tips. Symmetrical control was exhibited by the Liz-Marzán group through ultrasonic irradiation of the growth solution of gold nanodecahedra.[153] This mechanism ensures a continuous supply of energy needed to reduce Au(III) salt, ensuring simultaneous growth on each face, leading to monodispersion of the final product.

The role of the reducing and capping agents in the morphological formation of star-like shapes has been demonstrated as well. Early work by Sau and Murphy showed that branching AuNPs could be synthesized, along with prisms, rods, and cubes, by adjusting the synthetic parameters, mainly concentrations of reagents, appropriately.[154] Senthil Kumar *et al.* demonstrated that PVP molecules, in DMF, could not only reduce the gold in a gold halide solution, but also control the rate at which AuCl₄⁻ ions were reduced on the surface of pre-formed gold seeds.[126] The resulting gold nanostar morphology was dependent on the concentration of PVP, indicating that capping ligands previously shown to yield isotropic particles and non-branching anisotropic particles could be utilized in the synthesis of more complex morphologies under careful scrutiny.

In seed-based syntheses, a smaller seed diameter will yield AuNSs of smaller core size and reduced branch density. Interestingly, the ability to tune the LSPR of AuNSs by changing the $R_{reductant}$ value is not significantly affected by precursor seed size if the other reaction parameters are kept constant.[46] These results indicate a ruggedness of seed-based syntheses of AuNSs, allowing for some flexibility in achieving final morphological monodispersity regardless of initial seed size dispersity. By varying seed size from 3 to 35 nm, Khlebtsov *et al.* were able to tune the final AuNS size from 45 to 150 nm, yielding LSPR redshifts from 630 to 900 nm, respectively.[155] The resulting increase in core size resulted in an increased branch density as well.

AuNSs have also been tuned through careful consideration of reducing agent concentration. In a seedless, one-step reaction, AuNSs were synthesized by Good's buffer 4-(2-hydroxyethyl)-1-piperazinepropanesulfonic acid (EPPS).[156] Upon increasing the concentration of EPPS at a constant pH of 7.4 in the presence of a constant HAuCl₄ concentration the resulting morphologies transformed from quasispherical to short
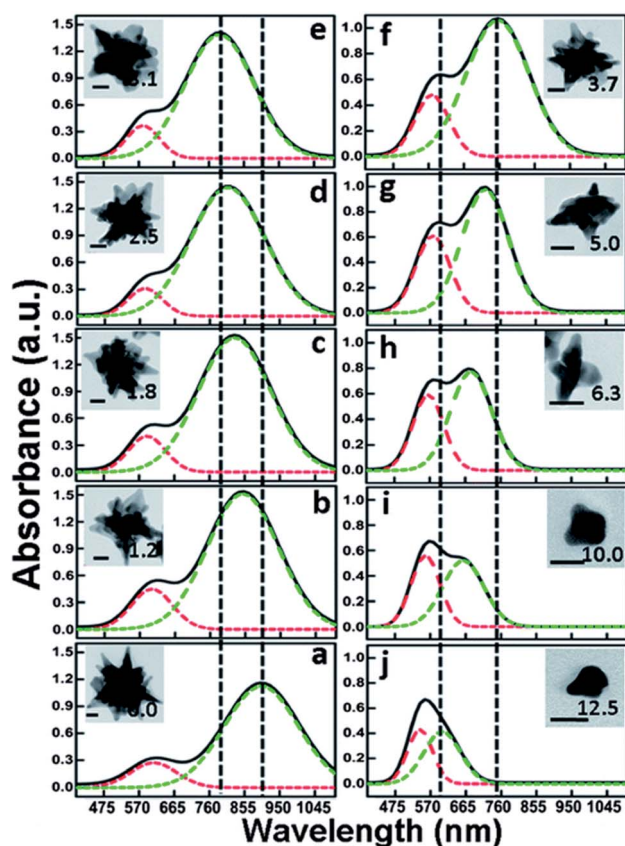

Fig. 11 Multiple Gaussian peak (dashed line) fitted optical absorption spectra for the as-prepared anisotropic gold nanostructures, for different NaOH concentrations (in mM) as mentioned. The corresponding gold nanostructure morphology is shown in the inset. The scale bar in all the images is equal to 20 nm; reprinted from ref. 149 with permission from The Royal Society of Chemistry.
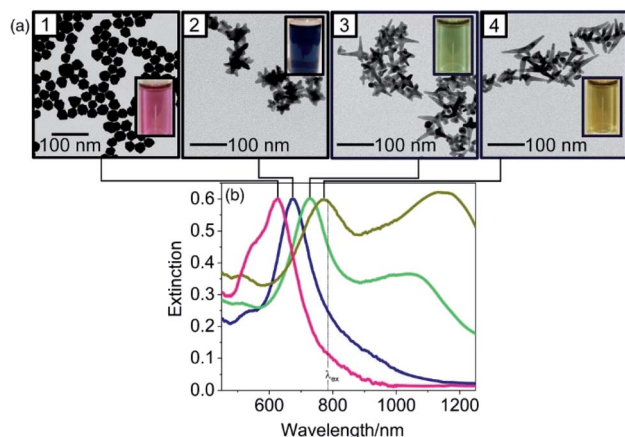
Fig. 12 The increased presence of a dual reducing and shape-directing agent in EPPS promotes the elongated branching structure by increasing the reduction rate of Au(III) while simultaneously allowing for additional ammine–Au shape-directing interactions. Reprinted with permission from ref. 156. Copyright © 2020 Wiley.

thorned particles to elongated-branched AuNSs (Fig. 12). EPPS, like many Good's buffers used in the synthesis of anisotropic nanosystems, acts as both a reducing agent and shape-directing surfactant primarily through interactions between its piperazine ring and the gold nanocrystals.[157] As these interactions increase between the ligand and the higher energy facets as EPPS concentration rises, the selective deposition of gold is more strictly directed towards lower energy facets resulting in the (111) directional branches. These results suggest that in the case of shape-directing reducing agents, rapid reduction and strong surface adsorption is a worthwhile strategy towards branching growth characteristic of stars.

6.2 Nanoflowers

Nanoflowers, having similar morphology characteristics to both nanostars and nanodendrites, can be distinguished by their pseudospherical cores and petal-like branches. AuNFs are of particular interest for their applications in optoelectronic devices, catalysis, and solar cells, but also for their distinct synthetic production.

Unlike many of the other branching AuNPs described in this review, flower-like AuNPs are often the result of self-assembled parent morphologies such as rod- and sheet-like nanostructures.[158] For example, gold nanosheets were synthesized through the UV-irradiation of HAuCl$_4$ in the presence of ethanolic PVP and AgNO$_3$.[159] While PVP is typically considered a nonreducing agent in the synthesis of gold nanostructures, under the influence of UV-light and Ag(I), reduction is possible. The strong interactions between PVP and the {100} facets of the Au crystal led to preferential growth along the {111} facets, leading to sheet morphologies. Subsequent centrifugation of the nanosheets resulted in a self-assembled nanoflower. The repeated washing steps remove excess PVP and bring together the nanosystems, increasing van der Waals attraction between the particles. The hydrophobic chains on the surface-adsorbed

PVP molecules and high surface energy of side–face and face–face alignments promote a side–side aggregation of the particles and the final flower morphology. This work suggests an advantage to the morphological control of AuNFs over their fellow branching nanoparticle counterparts; the flower-like structures may benefit from changes in the procedural steps that can affect the degree of aggregation of building blocks such as the aforementioned nanosheets.

Gold nanoflowers have also been synthesized using biological surfactants that, as insoluble in water, form vesicles as opposed to the micelles seen in traditional surfactants such as CTAB.[160] Cationic unilamellar vesicles formed by a bis(2-ethylhexyl) sulfosuccinate sodium salt (AOT) and CTAB solution can reduce HAuCl$_4$ without an additional reducing agent, but neither can reduce it by itself.[161] The resulting gold nanoclusters are able to be used as pseudo-seeds; the fast addition of ascorbic acid and Ag(I) ions results in structured platelet aggregates with a flower-like inner structure.

Vesicle-based syntheses of these flower-like structures is dependent on the "seed" solution undergoing formation at the time that the reducing agent is added.[162] The slow adsorption of the vesicle surfactant is overcome by the reducing power of AA, leaving certain crystal planes of the "seed" uncapped, leading to anisotropic growth and selective aggregation.

Although much of the present literature of AuNFs consists of the assembly of seed-like structures to form the resulting petal-like morphologies, there is interest in less tedious, one-pot syntheses. One such synthesis reduced HAuCl$_4$ with AA and utilized cetrimonium chloride (CTAC) as a capping ligand.[163] The AA causes a gradual reduction of the gold in a AuCl$_4$–CTA complex; the resulting gold nuclei aggregate until they reach a critical size which allows for free surfactant to bind onto the low energy (111) facets, a characteristic of ionic surfactants that leads to anisotropic growth on higher energy facets usually placated by capping ligands. As lower concentrations of Au are subsequently able to adsorb onto the (111) facets, divots are formed leading to hydrangea-like structures. Rather than varying seed-like precursors in order to tune the morphology of the final flower-like structures, one can resort to more traditional tuning techniques such as varying the concentrations of reagents, changing the solution pH, or temperature control.

The plasmonic properties of AuNFs are directly dependent on the size and width of their petals; as the sheet-like structures become thicker, the LSPR will tend to red-shift.[164–167] As such, researchers' attempts in tuning these nanosystems for specific applications should focus on the size adjustment on the petals themselves rather than particle size.

6.3 Urchins

Much like other multipod-esque gold nanostructures, urchin-like gold nanoparticles are of considerable interest due to an ability to tune the number, size, and length of spikes. Characterized by an extreme number of short, sharp thorns and subsequent numerous narrow voids, these features act as hot-spots for the lightning rod effect, as well as tuneable NIR plasmon bands.[168] As such, the formation and control of these, what

could be considered unwieldly, hierarchical structures is vital to their use. Wang *et al.* found that the rapid addition of excess mild reducing agents such as AA to an aqueous Au(III) solution caused a burst nucleation that can be further tailored to yield either spherical particles or branching urchins.[169] The presence of a capping agent such as bovine serum albumin (BSA) worked in tandem with the dehydroascorbic acid (DHA) formed and limited the initial gold seed growth to clusters, leading to the formation of isometric particles. In the absence of the additional capping agent, the rapid injection of AA yielded 10 nm particles which, due to high surface energy, aggregated quickly forming urchins with (111) facet nanogaps. Whereas slower reduction is necessary in the syntheses of other branching nanostructures, this work suggests that a morphological chaos of gold nanourchins is formed through uninhibited growth. As described previously in this review, methods towards kinetic control in the synthesis of gold nanosystems can be achieved through adjustments in the concentrations of seed precursors, reducing/capping agents, and thermal control, leading to many ways forward for the synthesis of similarly created urchin-like morphologies.

This hypothesis is further supported by a seed-mediated synthesis of gold urchins by the rapid reduction of Au(III) by H_2O_2 in the absence of an additional reducing agent.[57] Trace Ag(I) ions were used to tune particle shape, size and thorn length; as silver nitrate concentration increased the particles transformed from flower-like microspheres to urchins to morphologies similar to that of a nanopopcorn. Researchers found that the urchin-like morphologies were formed from small flower-like assemblies and that the thorns grew from the petals on the flowers: gold nanosheets with (111) basal planes.

Further work undertaken by the Odom group has shown the capabilities of various Good's buffers to facilitate the synthesis of Au urchins.[170] Through a seed-based method AuNPs were synthesized using each of the biocompatible EEPS, HEPES, and MOPS, respectively, as reducing and shape-directing agents. The authors found that the urchin morphology and the corresponding plasmonic properties could be manipulated through changes in R_{seed}, seed size, and pH. Interestingly, the group was able to conserve spike length and the corresponding LSPR wavelength, while increasing the seed size and thus the overall seed side. This suggests that, as with other branching morphologies synthesized through the use of Good's buffers, the anisotropic growth may be facilitated by a template-based method in which the reducing agent acts as a shape-directing agent as well.[171]

Gold nanourchins have also been produced by dual reducing agents. In a seed-mediated synthesis conducted by Cao *et al.*, hydroquinone and citrate were used in tandem to create, at high concentrations of hydroquinone, urchin morphologies with random spike growth on the {111}, {200}, {220} and {311} crystalline facets.[71] The pseudospherical particles formed at low hydroquinone concentrations may suggest selective facet targeting by reducing agents of different strengths, indicating dual-reduction options towards the tuneable synthesis of urchins. Li *et al.* also created gold nanourchins through the dual reduction of Au(III) by hydroquinone and sodium citrate
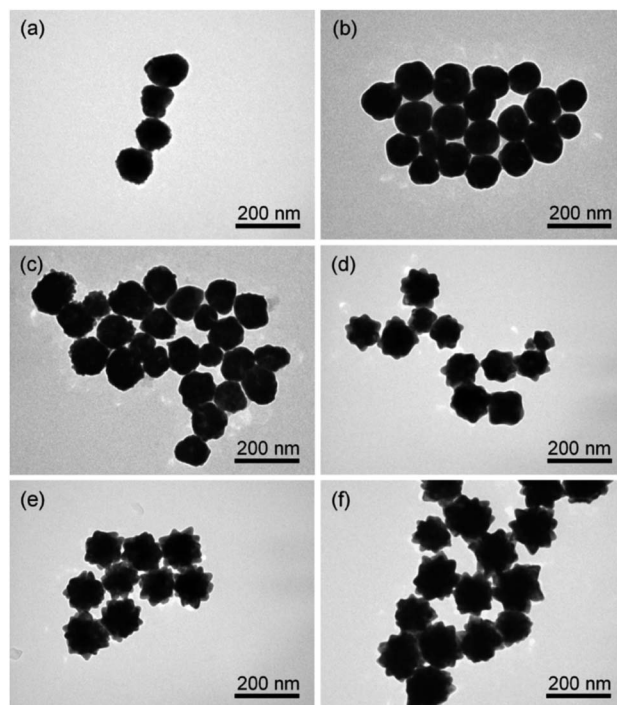

Fig. 13 Influence of hydroquinone amount on the morphologies of the as-prepared gold NPs. The amount of hydroquinone was altered from 50 (a), 100 (b), 120 (c), 150 (d), and 500 μL (e) to 1000 μL (f), while the amount of seeds, HAuCl₄, and sodium citrate was fixed at 50, 25, and 22 μL, respectively. Reprinted with permission from ref. 42. Copyright © 2011 American Chemical Society.

and observed that an increase in hydroquinone concentration resulted in urchin morphologies.[42] The high hydroquinone levels may directly have led to an increase in gold reactivity, promoting reduction of Au(I) to Au(0), fast nanoparticle growth, and anisotropy (Fig. 13).

Increasing the amount of seed precursor at constant Au(III) and reducing agent concentrations led to a lower Au(0) : seed ratio and resulted in further anisotropy. The disallowance of isotropic growth is likely due to the increased reducing agent : seed ratio; the excess of reducing agent is able to more efficiently saturate specific facets, inhibiting growth at those locations and promoting overgrowth at the facets that are less protected. This would be assumed to be a kinetically favourable process as the rapidly reduced Au(I) ions are selectively deposited on open faces leading to the observed thorn-like protrusions.

6.4 Dendrites

One great advantage exhibited by the morphology of branched gold nanoparticles is an increase in surface area caused by the protruding appendages. Dendritic gold nanoparticles encapsulate this quality perhaps better than any of the other branched morphologies as their shapes are defined by hyperbranching overgrowth; each branch protruding from the core contains many secondary and even tertiary branches. Pine tree, fern and other complex shapes are often observed and as such

the use of biotemplates in the synthesis of dendritic AuNPs is understandably appropriate.

Seo *et al.* utilized the M13 virus' cationic carboxylate groups for nucleation and growth of Au dendrites through electrochemical co-deposition.[172] Interactions between the gold salt precursor $AuCl_4^-$ and the NH_2 groups result in amminechloride complexes that, when a constant -0.2 V potential is applied, witness reduction of Au(III) to Au(0). Stabilization and growth of these zero-valent gold atoms is coordinated by the carboxylate groups of the M13 virus. The resulting anisotropic growth is dependent on the slow reduction of Au(III) as it is released from the ammine-chloride, the rate of which may be able to be controlled by adjusting the electrical potential. This method of morphological control is unique to dendritic structures and is a relatively facile method towards tunability.

This electrochemical behaviour was also observed by Rafatmah *et al.* in the electrodeposition synthesis of Au dendrites onto paper fibres to be used as catalysts.[173] As anisotropic growth will often occur under conditions far from equilibrium, sufficiently negative applied potentials will cause dendrite formation. It is understandable to assume then that higher deposition potential values would lead to denser gold nanostructures. The authors demonstrated that increasing the concentration of $HAuCl_4$ led to significantly higher branching which may be a method utilized for size control.

6.5 Multipods

Branched gold nanoparticles consisting of multiple rounded arms protruding from the core have been investigated as well. These nanomultipods, consisting of three or more branching structures, are differentiated from other morphologies such as nanostars and urchins by thicker spikes and duller tips. Gold tripods and tetrapods were among the first branching AuNPs synthesized through a CTAB and AA synthesis.[9] Interestingly, some of these multipods consist of quasispherical-like branches attached to an anisotropic core rather than arm-like protrusions and have been utilized for *in vivo* photoacoustic imaging.[174] Symmetrical-plane gold tripods are particularly difficult to grow through traditional methods as they require specific growth from every other ⟨110⟩ direction, but through electroless plating methods gold nanospheres can undergo morphological evolution to tripods using periodic double gyroid nanoporous templates.[175] This underexplored method of multipod synthesis presents an interesting approach towards the creation of branching gold nanoparticles; because control of isotropic nanoparticle growth is often significantly higher than their anisotropic counterparts greater final morphological control may be able to be achieved.

Nanotetrapods have been synthesized using a variety of biological Good's buffers including HEPES, EPPS, and 3-(*N*-morpholino)propanesulfonic acid (MOPS).[115,176,177] Morphological control differs between these buffers based on their carbon chain structures. For example, the additional methylene group between the piperazine ring and the sulfonic acid group in EPPS compared to HEPES slows the reduction rate and increases monodispersity, yielding tetrapods at a 75% rate.[176] While

a kinetically slower growth process in gold nanosystems produced by HEPES has been demonstrated to yield gold nanostars, the EPPS-reduced nanosystems retain the broad tips indicative of multipods.[80,178] The resulting monodispersity presents an advantage to this Good's buffer-based synthesis over its nanostar counterparts. While the broadened tips do decrease the intensity of electronic "hot spots" desired for use in applications such as SERS the consistent structure leads to better control over the plasmon properties.

The morphological tuning of gold tetrapods from shuriken-like structures has been described in a recent study by Zhang *et al.*[179] Synthesized in DMF, the uniquely shaped structures were synthesized through the use of diethylamine, a capping agent that selectively adsorbed to the {110} facets, allowing preferential growth in the [110] directions. As temperature increased, the shape of the nanosystems changed from large core, sharp tipped structures to tetrapods with broad, rounded branches (Fig. 14). The temperature dependence of the tetrapods may be due to competition between the rate at which gold is

Fig. 14 (a–d) TEM images of the Au nanoshurikens with tips of different lengths and sharpness obtained from a typical synthesis at temperatures of 60, 80, 100 and 150 °C, respectively. The reaction times were 90, 40, 10 and 10 min, respectively. Inset: Au nanoshurikens standing on their lateral sides. (e) Corresponding UV-vis-near infrared (NIR) spectra of the Au nanoshurikens. Right: Digital photographs of the respective sols of the Au nanoshurikens. Reprinted from ref. 179 with permission from The Royal Society of Chemistry.

preferentially deposited on the branch tips *versus* its migration to lower energy facets.[180,181] At low temperature, a slight advantage lies with deposition over migration, which leads to the observed sharp tips and broad core. As temperature increases, the rate at which gold is deposited onto the tips of the core must be significantly higher than the rate at which it diffuses onto the lower energy facets, resulting in the broad tipped tetrapods observed in Fig. 14d. This work in particular shows the great control that temperature can have on tuning the morphologies of branching nanoparticles.

Additional highly branched AuNPs with rounded tips have been synthesized and morphologically controlled in a variety of procedures. Wang *et al.* found that gold nanorods could be used as seeds to generate a variety of morphologies by altering both the aspect ratio of the rods and the reduction rate of AA by pH adjustments.[177] Biomolecules such as dendritic peptides containing NH_2 termini such as L-glutamic acid derivatives were able to form penta- and hexa-pods through kinetic control of the reaction by increasing reductant concentration or pH.[182,183]

6.6 Miscellaneous shapes

Many other branching gold nanoparticles exist that cannot be strictly regulated to one of the previously described categories. Gold nanocrosses were synthesized through reduction of $HAuCl_4$ by various copper species in the presence of a shape directing agent, oleylamine.[184] Morphological control was obtained by manipulating the reduction rate by copper species selection, either Cu(I), Cu nanowires, or their combination.

Li *et al.* utilized hollow spiked gold nanoshells for chemo-thermal antitumor therapy.[185] The chitosan-functionalized-liposome-based shells were synthesized by locking $AuCl_4^-$ anions with charged ammonium species from chitosan, which when reduced formed a branched gold coating. The overgrowth of gold nanorods through kinetic control by CTAC and selective surface blocking by Ag UPD was able to lead to gold nanoarrows consisting of two pyramidal heads and a four-wing shaft.[30]

Chitosan was also utilized as both a templating and a capping agent to synthesize gold nanoraspberries for photothermal therapy.[186] Utilizing a silver-mediated ascorbic acid-reduced synthesis, the templating role of chitosan was employed to selectively alter the size of the resulting particles. While many changes in reaction conditions that affect particle size will result in significant morphological changes as well, decreasing the chitosan concentration resulted in a decreased size of the particles while maintaining their berry-like shape. The researchers attribute this scaled-down ability to the active templating role exhibited by chitosan.

7. Applications

7.1 Surface-enhanced Raman spectroscopy

While most photons readily experience elastic Rayleigh scattering during light scattering, only about 1 in 10 million photons undergo Raman scattering, an inelastic exchange of energy with the scattering material.[187] Surface-enhanced Raman scattering (SERS) takes advantage of electromagnetic

enhancements due to the LSPRs of nanoparticles and is capable of providing complete vibrational blueprints of the analyte molecules.[147] This enhancement is caused by the ability of AuNPs to act as nanolenses, channelling deep visible or NIR wavelengths to subwavelength dimensions.[188] The effect of plasmonic nanoparticle structure on SERS depends on the chemical and electromagnetic effects.

The chemical enhancement is measured by the increased Raman cross-section of an analyte adsorbed onto the nanoparticle *versus* that of the free analyte.[189] The Raman cross-section of a AuNP-bound analyte can be preferentially increased if the excitation laser wavelength is resonant with the charge-transfer state of the nanoparticle–molecule complex, a property dependent on both the plasmon resonance of the nanoparticle and the molecular resonance of the analyte.[190] For the nanoparticle, extinction intensity at the common SERS excitation wavelength of 785 nm can help enhance this state. As branched AuNPs often demonstrate NIR absorption due to their core protrusions that are tuneable through branch elongation or shortening, narrowing or thickening, they are excellent candidates for SERS (Fig. 15).[191]

Branching AuNPs also lend themselves to SERS due to their preferred electromagnetic effects. An increased number of tips, valleys and edges give rise to the large EF areas, or "hot spots" necessary for successful use in SERS. As described previously, tuning of branching AuNP morphologies can lead directly to an increased number of protrusions and subsequent tips. The ability to introduce additional "hot spots" through synthetic adjustments in morphologies such as urchins and flowers

Fig. 15 (A) SEM and TEM images of the HGNs prepared by using different amounts of $HAuCl_4$ (50 mM) at 60 °C: (a and e) 0.1 mL, (b and f) 0.2 mL, (c and g) 0.4 mL, and (d and h) 0.6 mL, while the amount of dopamine hydrochloride (53 mM) was fixed at 2.0 mL. (B) Vis–NIR absorbance spectra of the corresponding HGNs in part (A). (C) The Raman spectra of 4-MBA labelled HGNs. Reprinted with permission from ref. 191. Copyright © 2018 Xiaowei Cao.

shows key advantages to the SERS capabilities of these structures.

To this end, branching AuNPs have been used extensively for SERS applications.[192,193] While top-down synthetic methods of SERS substrates, such as electron beam lithography and focused-ion beam lithography, are capable of producing highly reproducible materials, the high cost and limited tunability, as well as inability to synthesize anisotropic AuNPs make them less attractive than bottom-up methods.[194–196] However, the use of such AuNPs in SERS-based applications may require a "sandwich architecture"; nanoparticles are positioned such that there is a narrow gap between them and a plasmonic film allowing for realization of the quantum confinement effect.[197,198] Indrasekara *et al.* recognized and sought to improve on the disadvantages of the "sandwich architecture", primarily a limit on the sensitivity of the application.[192] Tuneable AuNSs and AuNPs were synthesized through a seed-, AgNO$_3$-, and AA-based method. The authors observed that the greater the plasmon peak maximum overlap with the 785 nm excitation wavelength, the greater the SERS enhancement. The species were able to detect analytes at concentrations as low as 1 pM and boasted an enhancement factor of 10^9, all without taking advantage of induced quantum confinement effects, but rather direct interactions between the nanoparticles and the analytes.

The surface characteristics of the branching AuNPs used in SERS applications may play as significant a role as their surface plasmon resonances. By synthesizing a series of increasingly branching gold nanoparticles through a thiol-driven arrested growth method, Meng *et al.* were able to quantify the effect that the sharp protrusions in their nanostar morphologies had on the resulting SERS effectiveness.[199] SERS spectra were measured directly from the various 4-mercapto-benzoic-acid-capped AuNP samples, including rough, spherical AuNPs and highly branching AuNSs. The authors found the SERS intensity from the AuNS solution to be three times that of the AuNP solution. This preferential increase in the SERS activity can understandably be attributed to the increased surface area due to long branching protrusions as well as the "lightning rod" effect of the sharp tips.

It is the complexity of branched gold nanoparticle morphologies that allows for such a wide breadth of applications. However, it is these intricate particle shapes that introduce a degree of difficulty in identifying appropriate surface functionalization. The Fabris group has identified an approach to determine optimal conditions for an anisotropic nanoparticle-based SERS system.[200] By coating gold nanostars with a silica layer in tandem with ATP as a Raman reporter molecule the researchers were able to measure the SERS response as the silica encasing was selectively etched away. This process allows for identification of the most efficient combination of surface functionalization and morphological structure. In the case of the surfactant-free gold nanostars synthesized in this experiment for example, the group was able to determine a correlation between the intensity of the stars' morphology and the SERS signal enhancement. Their work suggests that such a process could be used to experimentally determine such correlations in other branching gold particles as well.

Consideration of the morphological characteristics of branching AuNPs and the ability to tune them through careful experimental consideration gives way to a direct pathway for greater SERS enhancement.

7.2 Catalysis

Traditionally, when considering noble metal nanoparticles as catalysts, small, <20 nm spherical particles with high surface-to-volume ratios have been selected as they exhibit higher catalytic activity. As with other applications, branching AuNPs overcome the size limitation by increasing not only the exposed surface but also the number of activation sites.[132] The abundant defects and high surface energies from the edges and tips of branches increase the local electron density and, accordingly, reactivity in morphologies such as stars, flowers, and urchins. In order to examine morphological and size trends in the catalytic ability of gold nanomaterials to reduce 4-nitrophenol (4-NP) to 4-aminophenol (4-AP) in excess NaBH$_4$, Ma *et al.* recently synthesized spherical and branching AuNPs of various sizes.[201] Spherical AuNPs of 4, 16, 40, and 80 nm diameter showed an expected inverse relationship with size; the 4 nm particles completed the reduction of 4-NP in within 2 min while the 16 nm and 40 nm AuNPs took 12 and 15 min, respectively. Alternatively, as the size of the branching AuNPs increased from 40 nm to 117 nm the larger core size and branch lengths cause reduction time to decrease from 1.5 min to 0.6 min. The higher catalytic activity can be attributed to the highly energetic surfaces of the sharp tips.[26] As control over branch length, density, and sharpness becomes more facile through greater understanding of the driving forces behind morphological changes, catalytic capabilities should increase as well.

A recent comprehensive review by Priecel *et al.* has described the advantages of branched AuNPs for electrocatalytic reactions.[202] The authors attribute the effectiveness to the structure's ability to utilize the observed enhanced electric fields produced at edges and tips. The anisotropic gold nanoparticle-catalysed oxidation of methanol by nanoprisms, nanoperiwinkles, and nanoflowers immobilized on porous silicate networks was compared to that of spherical nanoparticles.[203] Catalytic activity was observed to increase not with an increase in surface area but rather as more high-index facets were observed. Understandably, the periwinkle and flower shapes were significantly more efficient than prisms and spherical particles. This trend was observed in dendrite-supported electrodes as well; the greater the high-index facets the stronger the electric field enhancement and the more efficient the catalytic ability. The directed synthesis of branched gold nanoparticles with the intention of propagating high-index facets amongst numerous edges and tips should drive the future of metal nanoparticle-based catalysis.

7.3 Photothermal and photodynamic therapy

The desire for non-invasive, collateral-free treatment of cancerous cells has directed research of nanoparticle-mediated

photothermal therapy (PTT). The photothermal heating process of gold nanomaterials was described in detail by Link *et al.*[204] Absorption of NIR light by gold nanosystems causes an excitation of plasmon band free electrons. The resulting hot electron pulse undergoes rapid cooling through collisions with the gold framework and instantly heats the nanosystems to temperatures in the thousands of degrees. That heat is then transferred to the surrounding cells and can induce hyperthermia, leading to cell death.

Understandably, the absorption of NIR light is a key parameter in choosing an appropriate nanomaterial. Gold nanostars in particular are intriguing materials for PTT as their LSPR can be selectively red-shifted into the NIR as the core size, number of branches, length of branches, and sharpness increase, morphological changes that can be selectively changed through procedural alterations.[205] Pallavicini *et al.* synthesized seed and silver-mediated gold nanostars reduced by ascorbic acid that showed two intense, photothermally active LSPRs.[206] 250 μL of 4 mM $AgNO_3$ and 5 mL of 1 mM $HAuCl_4$ were added to 5 mL of a 0.2 M solution of TritonX-100. 140–400 μL ascorbic acid was subsequently added and reduction was observed by a colour change in solution from yellow to clear, followed by an addition of a TritonX-100-capped gold seed solution. At least one branch from the resulting stars is formed at an angle to the others, leading to the two distinct NIR peaks, tuneable based on the concentration of ascorbic acid, at 670 and 1170 nm, 795 and 1450 nm, or 960 and 1590 nm. Upon irradiation of the stars in water with a suitable laser, a change in the environmental temperature of 7 and 12 K was observed at laser powers of 50 and 100 mW, respectively.

Photodynamic therapy (PDT), an alternative treatment that has proven effective for numerous cancers, is a promising landscape for the field of nanotheranostics to expand. In brief, PDT involves the delivery of photosensitizers (PSs) to a tumour site, followed by activation by illumination with NIR or visible light.[207] The photochemical reaction generates singlet oxygen, which induced apoptosis and necrosis in the tumour cells, by transferring the absorbed energy to normal tissue oxygen. Treatment of deep-tissue tumours with PDT is normally challenging; penetration of such tissue depth is exclusive to NIR light, but very few PSs are activated by such low energy.

As such, multi-branched gold nanoechinuses (AuNEs) were synthesized through a seed- and silver-mediated method, utilizing a double chain CTAB (DC14TAB) surfactant and ascorbic acid as a reducing agent. The DC14TAB surfactant was removed through a water and methanol wash, allowing for coating with PS Lipofectamine 2000 (LP-2000) which formed surface-coated bilayers.[208] The AuNEs showed extinction intensity well into the NIR, up to 1700 nm, molar extinction coefficients 7–9 times higher than those of conventional organic dyes and photosensitizers and 3–4 orders high than those of other gold nanoparticles (Fig. 16). The tunability of other branching AuNPs into the second biological window has been demonstrated, indicating that their use as upconversion nanoparticles (UCNPs) is a promising field.

Further work into the tunability of a second NIR plasmon band should be of great interest to researchers moving forward
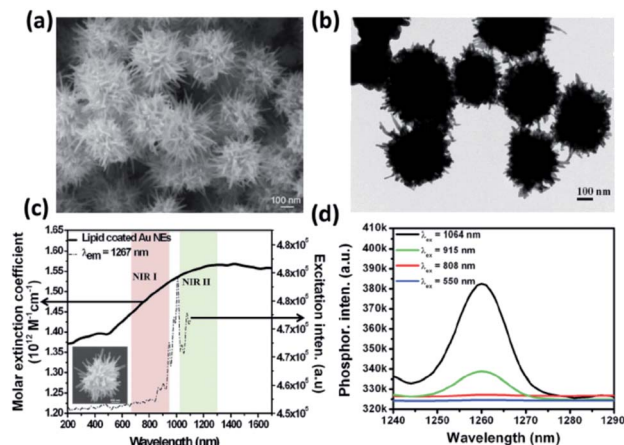

Fig. 16 Characterization and optical properties of AuNEs. (a and b) Scanning electron microscope (SEM) and transmission electron microscope (TEM) images of the as-synthesized AuNEs. (c) UV/Vis/NIR absorption spectrum (black solid line) and excitation spectrum (black dashed line) for singlet oxygen phosphorescence of lipid-coated AuNEs ($\lambda_{em} = 1267$ nm). The NIR I and II biological windows are indicated by the pale pink and green bars. The inset shows the SEM image of a single AuNE. (d) Singlet oxygen phosphorescence emission spectra sensitized by lipid-coated AuNEs at 550, 808, 915, and 1064 nm excitation wavelengths. Reprinted with permission from ref. 208. Copyright © 2014 Wiley.

as its biomedical applications could serve to elevate the use of noble metal nanoparticles in therapeutic settings to practical heights.

While morphology and application are undeniably linked, a final impressive feat of branching AuNPs is their multifunctionality. The Vo-Dinh group exemplified this by their creation of quintuple-modality AuNSs.[209] By creating a nanomaterial with an SPR within the NIR tissue optical window and functionalizing the surface with a traditional magnetic resonance imaging (MRI) contrast agent (Gd-DOTA) and SERS reporter (*para*-mercaptobenzoic acid), the researchers were able to create a singular platform for five different applications: SERS, MRI, computed tomography, two-photo-luminescence imaging and PTT. The absolute flexibility of such nanoparticle platforms should lend to their continued exploration.

7.4 Biosensing

Colorimetric-based assays for biosensing rooted in gold nanomaterials have gained traction due to the nanomaterials' ability to act as a colorimetric assay upon aggregation and etching. As nanomaterials aggregate, LSPR wavelengths will shift, allowing for robust point of care (POC) uses, which can be further confirmed if necessary by TEM or surface plasmon resonance imaging.[210,211] By utilizing the tunability of branching AuNPs, the LSPR maxima can be red- or blue-shifted such that the colour change upon aggregation is drastic enough to be discerned by the naked eye. Additionally, the easy functionalization of gold nanoparticle surfaces allows a wide array of detection techniques. For example, aggregation between CTAB-capped gold nanostars, which is usually prevented by the

positive charge on the ligand, can be induced by interactions with negatively charged cell walls of target bacteria such as *Staphylococcus aureus*. Verma *et al.* observed that such stars in the presence of *S. aureus*, DMPC, DMPE, and DMPG will selectively aggregate in the presence of only the negatively charged biochemicals: *S. aureus* DMPG liposome.[87] These nanostars in a water or saline solution display a deep blue colour and a corresponding ~580 nm LSPR maximum with little extinction intensity in the NIR. Upon injection of the negatively charged bacteria the AuNSs aggregate, causing the loss of the distinctive 580 nm LSPR caused by Mie scattering and displaying absorbance in the NIR instead. The colour of solution shifts from a deep blue to gray or colourless depending on bacteria concentration and is evidence of a robust POC device for *S. aureus* detection.

7.5 Drug delivery

The high biocompatibility and surface functionalization of AuNPs make them intriguing platforms for drug delivery. Along with PDT/PTT functionality, the increased surface area of branched AuNPs allows for a greater drug-load than their spherical counterparts. Agarwal *et al.* found that mammalian epithelial and immune cells preferentially internalize large hydrogel nanodiscs and nanorods as opposed to smaller spherical particles.[212] The researchers found that for successful cellular uptake, the particle morphology must find balance between two oppositely driving forces: while larger sized particles provide increased surface areas for greater adhesion forces between the particles and cell membranes they also increase the strain energy required for the cell membrane to bend around the particle. Branching AuNPs with high surface area and relatively low volume such as flowers and urchins should toe the line between the two parameters.

Recently, AuNFs and AuNUs functionalized with large neutral amino acid transporter 1 (LAT-1) targeting ligands, L- and D-DOPA, were used for uptake into breast cancer tumours and across the blood–brain barrier (BBB).[72,213] Ong *et al.* synthesized AuNFs through a seed mediated method in which the Au(III) salt and mPEG thiol were added to a 14 nm seed solution, followed by addition of L-DOPA at room temperature.[213] The resulting 90 nm AuNFs showed sufficient uptake into brain endothelial cells. Based on the amount of contact between the particle spikes and the plasma membrane, it may be the morphology of the particles itself that heps induce endocytic entry and facilitate BBB transport. This advantage shows the great benefit of carefully shaping control of these nanosystems.

8. Conclusions

As efforts toward noble metal nanoparticle synthesis continue to move forward, researchers have shown ever increasing control over the morphology that so dictates their application. By careful experimental examination, the metal frameworks of branching gold nanoparticles have been shown to be tailorable. As the optical and electronic properties of materials are directly connected to their morphologies this advantages does not simply stop at changing the size and shape of nanoparticles but at advancing the practical fields in which they are applied as well.

The published literature has shown that the tunability of branching gold nanoparticles is not only possible but also facile. However, the parameters that can lead to careful modification of the metallic frameworks of gold nanoparticles are not yet completely discovered nor understood. It is believed that a constant pursuit of this knowledge will not only open additional synthetic pathways for modifications of gold nanomaterials but will help expand the understanding of the fundamental nanoparticle nucleation and growth processes as well.

Conflicts of interest

There are no conflicts to declare.

References

1 M. Faraday, *Philos. Trans. R. Soc. London*, 1857, 147.
2 P. P. Edwards and J. M. Thomas, *Angew. Chem., Int. Ed.*, 2007, **46**, 5480–5486.
3 R. Sardar, A. M. Funston, P. Mulvaney and R. W. Murray, *Langmuir*, 2009, **25**, 13840–13851.
4 S. E. Lohse and C. J. Murphy, *Chem. Mater.*, 2013, **25**, 1250–1261.
5 T. H. Ha, H.-J. Koo and B. H. Chung, *J. Phys. Chem. C*, 2007, **111**, 1123–1130.
6 S. E. Skrabalak, J. Chen, Y. Sun, X. Lu, L. Au, C. M. Cobley and Y. Xia, *Acc. Chem. Res.*, 2008, **41**, 1587–1597.
7 J. Zhang, M. R. Langille, M. L. Personick, K. Zhang, S. Li and C. A. Mirkin, *J. Am. Chem. Soc.*, 2010, **132**, 14012–14014.
8 Y. Sun, B. Mayers and Y. Xia, *Adv. Mater.*, 2003, **15**, 641–646.
9 S. Chen, Z. L. Wang, J. Ballato, S. H. Foulger and D. L. Carroll, *J. Am. Chem. Soc.*, 2003, **125**, 16186–16188.
10 L. Fabris, *J. Phys. Chem. C*, 2020, **124**, 26540–26553.
11 L. M. Liz-Marzán, *Langmuir*, 2006, **22**, 32–41.
12 S. Wang, P. Huang, L. Nie, R. Xing, D. Liu, Z. Wang, J. Lin, S. Chen, G. Niu, G. Lu and X. Chen, *Adv. Mater.*, 2013, **25**, 3055–3061.
13 S. K. Dondapati, T. K. Sau, C. Hrelescu, T. A. Klar, F. D. Stefani and J. Feldmann, *ACS Nano*, 2010, **4**, 6318–6322.
14 E. N. Esenturk and A. R. H. Walker, *J. Raman Spectrosc.*, 2009, **40**, 86–91.
15 S. A. Lone and K. K. Sadhu, *Bioconjugate Chem.*, 2019, **30**, 1781–1787.
16 W. A. El-Said, T.-H. Kim, H. Kim and J.-W. Choi, *Biosens. Bioelectron.*, 2010, **26**, 1486–1492.
17 L.-X. Chen, J.-J. Lv, A.-J. Wang, H. Huang and J.-J. Feng, *Sens. Actuators, B*, 2016, **222**, 937–944.
18 F. Xu, W. Shang, G. Ma, Y. Zhu and M. Wu, *Sens. Actuators, B*, 2021, **326**, 128968–128975.
19 O. M. Bakr, B. H. Wunsch and F. Stellacci, *Chem. Mater.*, 2006, **18**, 3297–3301.

20 C. Kohout, C. Santi and L. Polito, *Int. J. Mol. Sci.*, 2018, **19**, 3385–3414.

21 S. Yu, H. Li, G. Li, L. Niu, W. Liu and X. Di, *Talanta*, 2018, **184**, 244–250.

22 N. A. Saltykova, O. L. Semerikova and N. G. Molchanova, *Russ. J. Electrochem.*, 2007, **43**, 863–869.

23 R. D. Vais, N. Sattarahmady, K. Karimian and H. Heli, *Sens. Actuators, B*, 2015, **215**, 113–118.

24 B. R. Danger, D. Fan, J. P. Vivek and I. J. Burgess, *ACS Nano*, 2012, **6**, 11018–11026.

25 K. Zhang, J. I. Cutler, J. Zhang, D. Zheng, E. Auyeung and C. A. Mirkin, *J. Am. Chem. Soc.*, 2010, **132**, 15151–15153.

26 S. Choi, Y. Moon and H. Yoo, *J. Colloid Interface Sci.*, 2016, **469**, 269–276.

27 S. Cohen-Pope, J. R. Crockett, M. Wang, K. Flynn, A. Hoff and Y. Bao, *J. Mater. Chem. C*, 2020, **8**, 12427–12436.

28 H. Parab, C. Jung, M.-A. Woo and H. G. Park, *J. Nanopart. Res.*, 2011, **13**, 2172–2180.

29 M. Liu, *Acta Phys.-Chim. Sin.*, 2018, **34**, 733–734.

30 Q. Wang, Z. Wang, Z. Li, J. Xiao, H. Shan, Z. Fang and L. Qi, *Sci. Adv.*, 2017, **3**, e1701183.

31 J. E. Ortiz-Castillo, R. C. Gallo-Villanueva, M. J. Madou and V. H. Perez-Gonzalez, *Coord. Chem. Rev.*, 2020, **425**, 213489–213511.

32 S. D. Perrault and W. C. W. Chan, *J. Am. Chem. Soc.*, 2009, **131**, 17042–17044.

33 N. C. Bigall, T. Härtling, M. Klose, P. Simon, L. M. Eng and A. Eychmüller, *Nano Lett.*, 2008, **8**, 4588–4592.

34 N. G. Bastús, J. Comenge and V. Puntes, *Langmuir*, 2011, **27**, 11098–11105.

35 H. Yuan, W. Ma, C. Chen, J. Zhao, J. Liu, H. Zhu and X. Gao, *Chem. Mater.*, 2007, **19**, 1592–1600.

36 C.-H. Kuo and M. H. Huang, *Langmuir*, 2005, **21**, 2012–2016.

37 M. R. Langille, J. Zhang, M. L. Personick, S. Li and C. A. Mirkin, *Science*, 2012, **337**, 954–957.

38 S. Atta, M. Beetz and L. Fabris, *Nanoscale*, 2019, **11**, 2946–2958.

39 A. S. Barnard, N. P. Young, A. I. Kirkland, M. A. van Huis and H. Xu, *ACS Nano*, 2009, **3**, 1431–1436.

40 J. L. Elechiguerra, J. Reyes-Gasga and M. J. Yacaman, *J. Mater. Chem.*, 2006, **16**, 3906–3919.

41 A. S. De Silva Indrasekara, S. F. Johnson, R. A. Odion and T. Vo-Dinh, *ACS Omega*, 2018, **3**, 2202–2210.

42 J. Li, J. Wu, X. Zhang, Y. Liu, D. Zhou, H. Sun, H. Zhang and B. Yang, *J. Phys. Chem. C*, 2011, **115**, 3630–3637.

43 X. Meng, A. Baride and C. Jiang, *Langmuir*, 2016, **32**, 6674–6681.

44 Y. Wang, K. Sentosun, A. Li, M. Coronado-Puchau, A. Sánchez-Iglesias, S. Li, X. Su, S. Bals and L. M. Liz-Marzán, *Chem. Mater.*, 2015, **27**, 8032–8040.

45 Y. Liu, J. R. Ashton, E. J. Moding, H. Yuan, J. K. Register, A. M. Fales, J. Choi, M. J. Whitley, X. Zhao, Y. Qi, Y. Ma, G. Vaidyanathan, M. R. Zalutsky, D. G. Kirsch, C. T. Badea and T. Vo-Dinh, *Theranostics*, 2015, **5**, 946–960.

46 S. Barbosa, A. Agrawal, L. Rodríguez-Lorenzo, I. Pastoriza-Santos, R. A. Alvarez-Puebla, A. Kornowski, H. Weller and L. M. Liz-Marzán, *Langmuir*, 2010, **26**, 14943–14950.

47 J. Rodríguez-Fernández, J. Pérez-Juste, P. Mulvaney and L. M. Y. Liz-Marzán, *J. Phys. Chem. B*, 2005, **109**, 14257–14261.

48 J. A. Webb, W. R. Erwin, H. F. Zarick, J. Aufrecht, H. W. Manning, M. J. Lang, C. L. Pint and R. Bardhan, *J. Phys. Chem. C*, 2014, **118**, 3696–3707.

49 K. L. Kelly, E. Coronado, L. L. Zhao and G. C. Y. Schatz, *J. Chem. Phys. B*, 2003, **107**, 668–677.

50 F. Hao, C. L. Nehl, J. H. Hafner and P. Y. Nordlander, *Nano Lett.*, 2007, **7**, 729–732.

51 G. Maiorano, L. Rizzello, M. A. Mavindi, S. S. Shankarm, L. Martiradonna, A. Falqui, R. Cingolani and P. P. Pompa, *Nanoscale*, 2011, **3**, 2227–2232.

52 V. M. Kariuki, J. C. Hoffmeier, I. Yazgan and O. A. Sadik, *Nanoscale*, 2017, **9**, 8330–8340.

53 H. Yuan, C. G. Khoury, H. Hwang, C. M. Wilson, G. A. Grant and T. Vo-Dinh, *Nanotechnology*, 2012, **23**, 075102.

54 M. M. Phiri, D. W. Mulder and B. C. Vorster, *R. Soc. Open Sci.*, 2019, **6**, 181971–181980.

55 S.-S. Chang, C.-W. Shih, C.-D. Chen, W.-C. Lai and C. R. C. Wang, *Langmuir*, 1999, **15**, 701–709.

56 Y. Ling, J. X. Li, F. Qu, N. B. Li and H. Q. Luo, *Microchim. Acta*, 2014, **181**, 1069–1075.

57 A. Pangdam, K. Wongravee, S. Nootchanat and S. Ekgasit, *Mater. Des.*, 2017, **130**, 140–148.

58 H.-L. Wu, C.-H. Chen and M. H. Huang, *Chem. Mater.*, 2009, **21**, 110–114.

59 F. Hubert, F. Testard and O. Spalla, *Langmuir*, 2008, **24**, 9219–9222.

60 J. Pérez-Juste, I. Pastoriza-Santos, L. M. Liz-Marzán and P. Mulvaney, *Coord. Chem. Rev.*, 2005, **249**, 1870–1901.

61 C. J. Orendorff and C. J. Murphy, *J. Phys. Chem. B*, 2006, **110**, 3990–3994.

62 M. Liu and P. Guyot-Sionnest, *J. Phys. Chem. B*, 2005, **109**, 22192–22198.

63 W. Tong, M. J. Walsh, P. Mulvaney, J. Etheridge and A. M. Funston, *J. Phys. Chem. C*, 2017, 3549–3559.

64 M. L. Personick, M. R. Langille, J. Zhang and C. A. Mirkin, *Nano Lett.*, 2011, **11**, 3394–3398.

65 T. V. Tsoulos, S. Atta, M. J. Lagos, M. Beetz, P. E. Batson, G. Tsilomelekis and L. Fabris, *Nanoscale*, 2019, **11**, 18662–18671.

66 A. Ayeni, S. Alam and G. Kipouros, *J. Mater. Sci. Chem. Eng.*, 2018, **9**, 80–89.

67 T. S. Rodrigues, M. Zhao, T.-H. Yang, K. D. Gilroy, A. G. M. da Silva, P. H. C. Camargo and Y. Xia, *Chem.–Eur. J.*, 2018, **25**, 16944–16963.

68 J. Dong, P. L. Carpinone, G. Pyrgiotakis, P. Demokritou and B. M. T. Moudgil, *Kona*, 2020, **37**, 224–232.

69 N. E. Larm, J. B. Essner, K. Pokpas, J. A. Canon, N. Jahed, E. I. Iwuoha and G. A. Baker, *J. Phys. Chem. C*, 2018, **122**, 5105–5118.

70 Y. Lee and T. G. Park, *Langmuir*, 2011, **27**, 2965–2971.

71 X. Cao, Z. Wang, L. Bi and J. Zheng, *J. Chem.*, 2018, 9012645–9012657.

72 D. A. Gonzalez-Carter, Z. Y. Ong, C. M. McGilvery, I. E. Dunlop, D. T. Dexter and A. E. Porter, *Nanomedicine*, 2019, **15**, 1–11.

73 X.-L. Zhang, C. Zheng, Y. Zhang, H.-H. Yang, X. Liu and J. Liu, *J. Nanopart. Res.*, 2016, **18**, 174.

74 T. B. Demille, R. A. Hughes, N. Dominique, J. E. Olson, S. Rouvimov, J. P. Camden and S. Neretina, *Nanoscale*, 2020, **12**, 16489–16500.

75 H. Bao, T. Bihr, A.-S. Smith and R. N. Klupp Taylor, *Nanoscale*, 2014, **6**, 3954–3966.

76 W. Wang, Y. Pang, J. Yan, G. Wang, H. Suo, C. Zhao and S. Xing, *Gold Bull.*, 2012, **45**, 91–98.

77 X. W. Lou, C. Yuan and L. A. Archer, *Chem. Mater.*, 2006, **18**, 3921–3923.

78 A. J. Blanch, M. Döblinger and J. Rodríguez-Fernández, *Small*, 2015, **11**, 4550–4559.

79 H.-L. Wu, C.-H. Kuo and M. H. Huang, *Langmuir*, 2010, **26**, 12307–12313.

80 W. Xi and A. J. Haes, *J. Am. Chem. Soc.*, 2019, **141**, 4034–4042.

81 J. D. S. Newman and G. J. Blanchard, *Langmuir*, 2006, **22**, 5882–5887.

82 E. G. Wrigglesworth and J. H. Johnston, *RSC Adv.*, 2017, **7**, 45757–45762.

83 Y. Xia, Y. Xiong, B. Lim and S. E. Skrabalak, *Angew. Chem., Int. Ed.*, 2009, **48**, 60–103.

84 T. K. Sau and C. J. Murphy, *Langmuir*, 2005, **21**, 2923–2929.

85 V. Berry, A. Gole, S. Kundu, C. J. Murphy and R. F. Saraf, *J. Am. Chem. Soc.*, 2005, **127**, 17600–17601.

86 C. L. Nehl, H. Liao and J. H. Hafner, presented in part at the *SPIE Optics + Photonics*, San Diego, 2006.

87 M. S. Verma, P. Z. Chen, L. Jones and F. X. Gu, *RSC Adv.*, 2014, **4**, 10660–10668.

88 P. Pallavicini, G. Chirico, M. Collini, G. Dacarro, A. Don à, L. D'Alfonso, A. Falqui, Y. Diaz-Fernandez, S. Freddi, B. Garofalo, A. Genovese, L. Sironi and A. Taglietti, *Chem. Commun.*, 2010, **47**, 1315–1317.

89 A. Kedia and P. Senthil Kumar, *RSC Adv.*, 2014, **4**, 4782–4790.

90 M. M. Vega, A. Bonifacio, V. Lughi, S. Marsi, S. Carrato and V. Sergo, *J. Nanopart. Res.*, 2014, **16**, 2729–2734.

91 V. Poonthiyil and V. B. Golovko, *Internet J. Nanotechnol.*, 2017, **14**, 337–347.

92 B. K. Jena and C. R. Raj, *Chem. Mater.*, 2008, **20**, 3546–3548.

93 M. Wei, N. Chen, J. Li, M. Yin, L. Liang, Y. He, H. Song, C. Fan and Q. Huang, *Angew. Chem., Int. Ed.*, 2012, **51**, 1202–1206.

94 F. Tian, J. Conde, C. Bao, Y. Chen, J. Curtin and D. Cui, *Biomater.*, 2016, **106**, 87–97.

95 J. Nam, S. Son and J. J. Moon, *Cell. Mol. Bioeng.*, 2017, **10**, 341–355.

96 S. W. Chee, S. F. Tan, Z. Baraissov, M. Bosman and U. Mirsaidov, *Nat. Commun.*, 2017, **8**, 1224–1231.

97 A. G. M. da Silva, T. S. Rodrigues, S. J. Haigh and P. H. C. Camargo, *Chem. Commun.*, 2017, **53**, 7135–7148.

98 J. K. Kim, T.-H. Park and D.-J. Jang, *J. Nanopart. Res.*, 2020, **22**, 305–315.

99 D. Zhu, Y. Liu, M. Liu, C. Liu, P. N. Prasad and M. T. Swihart, *J. Mater. Chem. B*, 2020, **8**, 5491–5499.

100 M. Pradhan, J. Chowdhury, S. Sarkar, A. K. Sinha and T. Pal, *J. Phys. Chem. C*, 2012, **116**, 24301–24313.

101 W. Ni, H. Ba, A. A. Lutich, F. Jäckel and J. Feldmann, *Nano Lett.*, 2012, **12**, 4647–4650.

102 X. Kou, W. Ni, C.-K. Tsung, K. Chan, H.-Q. Lin, G. D. Stucky and J. Wang, *Small*, 2007, **3**, 2103–2113.

103 S. Sitaula, M. R. Mackiewicz and S. M. Reed, *Chem. Commun.*, 2008, 3013–3015.

104 Z. Zhang, Z. Chen, D. Pan and L. Chen, *Langmuir*, 2015, **31**, 643–650.

105 T. Wen, H. Zhang, X. Tang, W. Chu, W. Liu, Y. Ji, Z. Hu, S. Hou, X. Hu and X. Wu, *J. Phys. Chem. C*, 2013, **117**, 25769–25777.

106 R. Zou, X. Guo, J. Yang, D. Li, F. Peng, L. Zhang, H. Wang and H. Yu, *CrystEngComm*, 2009, **11**, 2797–2803.

107 M. Lu, L. Su, Y. Luo, X. Ma, Z. Duan, D. Zhu and Y. Xiong, *Anal. Methods*, 2019, **11**, 4829–4834.

108 L. Zhang, W. Hou, Q. Lu, M. Liu, C. Chen, Y. Zhang and S. Yao, *Anal. Chim. Acta*, 2016, **947**, 23–31.

109 G. Weng, X. Dong, J. Li and J. Zhao, *J. Mater. Sci.*, 2016, **51**, 7678–7690.

110 H. Yuan, K. P. F. Janssen, T. Franklin, G. Lu, L. Su, X. Gu, H. Uji-i, M. B. J. Roeffaers and J. Hofkens, *RSC Adv.*, 2015, **5**, 6829–6833.

111 L. Rodríguez-Lorenzo, J. M. Romo-Herrera, J. Pérez-Juste, R. A. Alvarez-Puebla and L. M. Liz-Marzán, *J. Mater. Chem.*, 2011, **21**, 11544–11549.

112 P. P. Ghimire and M. Jaroniec, *J. Colloid Interface Sci.*, 2020, **584**, 838–865.

113 M. N. Sanz-Ortiz, K. Sentosun, S. Bals and L. M. Liz-Marzán, *ACS Nano*, 2015, **9**, 10489–10497.

114 K. Chandra, K. S. B. Culver, S. E. Werner, R. C. Lee and T. W. Odom, *Chem. Mater.*, 2016, **28**, 6763–6769.

115 H. Liu, Y. Xu, Y. Qin, W. Sanderson, D. Crowley, C. H. Turner and Y. Bao, *J. Phys. Chem. C*, 2013, **117**, 17143–17150.

116 D. H. M. Dam, K. S. B. Culver and T. W. Odom, *Mol. Pharm.*, 2014, **11**, 580–587.

117 D. H. M. Dam, K. S. B. Culver, I. Kandela, R. C. Lee, K. Chandra, H. Lee, C. Mantis, A. Ugolkov, A. P. Mazar and T. W. Odom, *Nanomedicine*, 2015, **11**, 671–679.

118 V. V. Hardikar and E. Matijević, *J. Colloid Interface Sci.*, 2000, **221**, 133–136.

119 R. Kumar, I. Roy, T. Y. Ohulchanskyy, L. N. Goswami, A. C. Bonoiu, E. J. Bergey, K. M. Tramposch, A. Maitra and P. N. Prasad, *ACS Nano*, 2008, **2**, 449–456.

120 A. M. Fales, H. Yuan and T. Vo-Dinh, *Langmuir*, 2011, **27**, 12186–12190.

121 A. Hernández Montoto, R. Montes, A. Samadi, M. Gorbe, J. M. Terrés, R. Cao-Milán, E. Aznar, J. Ibañez, R. Masot, M. D. Marcos, M. Orzáez, F. Sancenón, L. B. Oddershede and R. Martínez-Máñez, *ACS Appl. Mater. Interfaces*, 2018, **10**, 27644–27656.

122 S. Atta, S. Rangan and L. Fabris, *ChemNanoMat*, 2020, **5**, 1–6.

123 J. Watt, S. Cheong and R. D. Tilley, *Nano Today*, 2013, **8**, 198–215.

124 A. Kedia and P. Senthil Kumar, *J. Phys. Chem. C*, 2012, **116**, 1679–1686.

125 A. Kedia, H. Kumar and P. Senthil Kumar, *RSC Adv.*, 2015, **5**, 5205–5212.

126 P. Senthil Kumar, I. Pastoriza-Santos, B. Rodríguez-González, F. Javier García de Abajo and L. M. Liz-Marzán, *Nanotechnology*, 2007, **19**, 015606–015611.

127 Y. Qin, Y. Song, N. Sun, N. Zhao, M. Li and L. Qi, *Chem. Mater.*, 2008, **20**, 3965–3972.

128 M. Anouti, A. Mirghani, J. Jacquemin, L. Timperman and H. Galiano, *Ionics*, 2013, **19**, 1783–1790.

129 C.-H. Lin, S.-P. Ju, J.-W. Su and D.-E. Li, *Sci. Rep.*, 2020, **10**, 2090–2100.

130 D. V. Wagle, H. Zhao and G. A. Baker, *Acc. Chem. Res.*, 2014, **47**, 2299–2308.

131 E. R. Parnham, E. A. Drylie, P. S. Wheatley, A. M. Z. Slawin and R. E. Morris, *Angew. Chem., Int. Ed.*, 2006, **45**, 4962–4966.

132 H.-G. Liao, Y.-X. Jiang, Z.-Y. Zhou, S.-P. Chen and S.-G. Sun, *Angew. Chem., Int. Ed.*, 2008, **47**, 9100–9103.

133 F. A. Mahyari, M. Tohidi and A. Safavi, *Mater. Res. Express*, 2016, **3**, 095006–095019.

134 M. Tsuji, M. Hashimoto, Y. Nishizawa, M. Kubokawa and T. Tsuji, *Chemistry*, 2005, **11**, 440–452.

135 Y. Fang, Y. Ren and M. Jiang, *Colloid Polym. Sci.*, 2011, **289**, 1769–1776.

136 T. Krishnakumar, R. Jayaprakash, N. Pinna, V. N. Singh, B. R. Mehta and A. R. Phani, *Mater. Lett.*, 2009, **63**, 242–245.

137 V. K. T. Ngo, T. P. Huynh and D. G. Nguyen, *Adv. Nat. Sci.: Nanosci. Nanotechnol.*, 2019, **10**, 035016–035023.

138 R. Luque, A. M. Balu, J. M. Campelo, C. Gonzalez-Arellano, M. J. Gracia, D. Luna, J. M. Marinas and A. A. Romero, *Mater. Chem. Phys.*, 2009, **117**, 408–413.

139 J. M. Campelo, T. D. Conesa, M. J. Gracia, M. J. Jurado, R. Luque, J. M. Marinas and A. A. Romero, *Green Chem.*, 2008, **10**, 853–858.

140 S. Kundu, L. Peng and H. Liang, *Inorg. Chem.*, 2008, **47**, 6344–6352.

141 K. R. Brown, D. G. Walter and M. J. Natan, *Chem. Mater.*, 2000, **12**, 306–313.

142 J. Park, K. An, Y. Hwang, J.-G. Park, H.-J. Noh, J.-Y. Kim, J.-H. Park, N.-M. Hwang and T. Hyeon, *Nat. Mater.*, 2004, **3**, 891–895.

143 A. Silvestri, L. Lay, R. Psaro, L. Polito and C. Evangelisti, *Chem.–Eur. J.*, 2017, **23**, 9732–9735.

144 P. J. Kitson, M. H. Rosnes, V. Sans, V. Dragone and L. Cronin, *Lab Chip*, 2012, **12**, 3267–3271.

145 T. Ishizaka, A. Ishigaki, H. Kawanami, A. Suzuki and T. M. Suzuki, *J. Colloid Interface Sci.*, 2012, **367**, 135–138.

146 K. Sai Krishna, C. V. Navin, S. Biswas, V. Singh, K. Ham, G. L. Bovenkamp, C. S. Theegala, J. T. Miller, J. J. Spivey and C. S. S. R. Kumar, *J. Am. Chem. Soc.*, 2013, **135**, 5450–5456.

147 A. Guerrero-Martínez, S. Barbosa, I. Pastoriza-Santos and L. M. Liz-Marzán, *Curr. Opin. Colloid Interface Sci.*, 2011, **16**, 118–127.

148 S. M. Mousavi, M. Zarei, S. A. Hashemi, S. Ramakrishna, W.-H. Chiang, C. W. Lai and A. Gholami, *Drug Metab. Rev.*, 2020, **52**, 299–318.

149 A. Kedia and P. Senthil Kumar, *J. Mater. Chem. C*, 2013, **1**, 4540–4549.

150 Y. Liu, H. Yuan, F. R. Kersey, J. K. Register, M. C. Parrott and T. Vo-Dinh, *Sensors*, 2015, **15**, 3706–3720.

151 B. Zümreoglu-Karan, *J. Nanopart. Res.*, 2009, **11**, 1099–1105.

152 W. Niu, Y. A. A. Chua, W. Zhang, H. Huang and X. Lu, *J. Am. Chem. Soc.*, 2015, **137**, 10460–10463.

153 A. Sánchez-Iglesias, I. Pastoriza-Santos, J. Pérez-Juste, B. Rodríguez-González, F. J. García de Abajo and L. M. Liz-Marzán, *Adv. Mater.*, 2006, **18**, 2529–2534.

154 T. K. Sau and C. J. Murphy, *J. Am. Chem. Soc.*, 2004, **126**, 8648–8649.

155 B. Khlebtsov, E. Panfilova, V. Khanadeev and N. Khlebtsov, *J. Nanopart. Res.*, 2014, **16**, 2623–2634.

156 R. A. Harder, L. A. Wijenayaka, H. T. Phan and A. J. Haes, *J. Raman Spectrosc.*, 2020, 1–9.

157 J. Xie, J. Y. Lee and D. I. C. Wang, *Chem. Mater.*, 2007, **19**, 2823–2830.

158 B. I. Kharisov, *Recent Pat. Nanotechnol.*, 2008, **2**, 190–200.

159 L. Wang, G. Wei, C. Guo, L. Sun, Y. Sun, Y. Song, T. Yang and Z. Li, *Colloids Surf., A*, 2008, **312**, 148–153.

160 M. S. Bakshi, *Cryst. Growth Des.*, 2016, **16**, 1104–1133.

161 F. Liebig, R. Henning, R. M. Sarhan, C. Prietzel, M. Bargheer and J. Koetz, *Nanotechnol*, 2018, **29**, 185603–185610.

162 M. S. Bakshi, F. Possmayer and N. O. Petersen, *Chem. Mater.*, 2007, **19**, 1257–1266.

163 C. Y. Song, N. Zhou, B. Y. Yang, Y. J. Yang and L. H. Wang, *Nanoscale*, 2015, **7**, 17004–17011.

164 X. Huang, S. Tang, X. Mu, Y. Dai, G. Chen, Z. Zhou, F. Ruan, Z. Yang and N. Zheng, *Nat. Nanotechnol.*, 2011, **6**, 28–32.

165 X. Huang, S. Tang, B. Liu, B. Ren and N. Zheng, *Adv. Mater.*, 2011, **23**, 3420–3425.

166 M. Chen, B. Wu, J. Yang and N. Zheng, *Adv. Mater.*, 2012, **24**, 862–879.

167 R. Jin, Y. Cao, C. A. Mirkin, K. L. Kelly, G. C. Schatz and J. G. Zheng, *Science*, 2001, **294**, 1901–1903.

168 H. Yuan, C. G. Khoury, C. M. Wilson, G. A. Grant, A. J. Bennett and T. Vo-Dinh, *Nanomed*, 2012, **8**, 1355–1363.

169 X. Wang, D.-P. Yang, P. Huang, M. Li, C. Li, D. Chen and D. Cui, *Nanoscale*, 2012, **4**, 7766–7772.

170 R. M. Pallares, T. Stilson, P. Choo, J. Hu and T. W. Odom, *ACS Appl. Nano Mater.*, 2019, **2**, 5266–5271.

171 K. Chandra, V. Kumar, S. E. Werner and T. W. Odom, *ACS Omega*, 2017, **2**, 4878–4884.

172 Y. Seo, S. Manivannan, I. Kang, S.-W. Lee and K. Kim, *Biosens. Bioelectron.*, 2017, **94**, 87–93.

173 E. Rafatmah and B. Hemmateenejad, *Sens. Actuators, B*, 2020, **304**, 127335–127346.

174 K. Cheng, S.-R. Kothapalli, H. Liu, A. L. Koh, J. V. Jokerst, H. Jiang, M. Yang, J. Li, J. Levi, J. C. Wu, S. S. Gambhir and Z. Cheng, *J. Am. Chem. Soc.*, 2014, **136**, 3560–3571.

175 T.-Y. Tang, H.-L. Wang, C.-T. Yao, K.-C. Yang, R.-M. Ho and D.-H. Tasi, *Nanoscale*, 2018, **10**, 7352–7356.

176 J. Cai, V. Raghavan, Y. J. Bai, M. H. Zhou, X. L. Liu, C. Y. Liao, P. Ma, L. Shi, P. Dockery, I. Keogh, H. M. Fan and M. Olivo, *J. Mater. Chem. B*, 2015, **3**, 7377–7385.

177 C. Wang, T. Wang, Z. Ma and Z. Su, *Nanotechnol*, 2005, **16**, 2555–2560.

178 S. Saverot, X. Geng, W. Leng, P. J. Vikesland, T. Z. Grove and L. R. Bickford, *RSC Adv.*, 2016, **6**, 29669–29673.

179 L. Zhang, X. Sha, Q. Fan, L. Han, Y. Yin and C. Gao, *Nanoscale*, 2017, **9**, 17037–17043.

180 X. Xia, S. Xie, M. Liu, H.-C. Peng, N. Lu, J. Wang, M. J. Kim and Y. Xia, *Proc. Natl. Acad. Sci. U. S. A.*, 2013, **110**, 6669–6673.

181 Y. Xia, X. Xia and H.-C. Peng, *J. Am. Chem. Soc.*, 2015, **137**, 7947–7966.

182 G. Palui, S. Ray and A. Banerjee, *J. Mater. Chem.*, 2009, **19**, 3457–3468.

183 C. Wang, *Adv. Mater. Res.*, 2013, **785–786**, 484–487.

184 E. Ye, M. D. Regulacio, M. S. Bharathi, H. Pa, M. Lin, M. Bosma, K. Y. Win, H. Ramanarayan, S.-Y. Zhang, X. J. Loh, Y.-W. Zhang and M.-Y. Han, *Nanoscale*, 2016, **8**, 543–552.

185 L. Li, Y. Fu, Z. Xu, Z. Hao, Y. He, W. Gao and D. Gao, *J. Mater. Chem. B*, 2020, **8**, 5155–5166.

186 N. Gandra, C. Portz, S. Z. Nergiz, A. Fales, T. Vo-Dinh and S. Singamaneni, *Sci. Rep.*, 2015, **5**, 10311.

187 Z. Du, Y. Qi, J. He, D. Zhong and M. Zhou, *WIREs Nanomed. Nanobi*, 2020, e1672–e1687.

188 V. Amendola, R. Pilot, M. Frasconi, O. M. Maragò and M. A. Iatì, *J. Phys.: Condens. Matter*, 2017, **29**, 203002–203049.

189 M. Moskovits, *J. Raman Spectrosc.*, 2005, **36**, 485–496.

190 J. R. Lombardi and R. L. Birke, *J. Phys. Chem. C*, 2008, **112**, 5605–5617.

191 X. Cao, S. Chen, W. Li, J. Li, L. Bi and H. Shi, *AIP Adv.*, 2018, **8**, 105133–105143.

192 A. S. D. S. Indrasekara, S. Meyers, S. Shubieta, L. C. Feldman, T. Gustafsson and L. Fabris, *Nanoscale*, 2014, **6**, 8891–8899.

193 P. Ndokoye, J. Ke, J. Liu, Q. Zhao and X. Li, *Langmuir*, 2014, **30**, 13491–13497.

194 T. Wu and Y.-W. Lin, *Appl. Surf. Sci.*, 2018, **435**, 1143–1149.

195 W. Yue, Z. Wang, Y. Yang, L. Chen, A. Syed, K. Wong and X. Wang, *J. Micromech. Microeng.*, 2012, **22**, 125007–125015.

196 K. Suekuni, T. Takeshita, K. Sugano and Y. Isono, presented in part at the *2014 IEEE 27th International Conference on Micro Electro Mechanical Systems*, MEMS, San Francisco, CA, 2014.

197 R. Alvarez-Puebla, L. M. Liz-Marzán and F. J. García de Abajo, *J. Phys. Chem. Lett.*, 2010, **1**, 2428–2434.

198 L. Rodríguez-Lorenzo, R. A. Álvarez-Puebla, I. Pastoriza-Santos, S. Mazzucco, O. Stéphan, M. Kociak, L. M. Liz-Marzán and F. J. García de Abajo, *J. Am. Chem. Soc.*, 2009, **131**, 4616–4618.

199 X. Meng, J. Dyer, Y. Huo and C. Jiang, *Langmuir*, 2020, **36**, 3558–3564.

200 S. Atta, T. V. Tsoulos and L. Fabris, *J. Phys. Chem. C*, 2016, **120**, 20749–20758.

201 T. Ma, W. Yang, S. Liu, H. Zhang and F. Liang, *Catalysts*, 2017, **7**, 38–47.

202 P. Priecel, H. Adekunle Salami, R. H. Padilla, Z. Zhong and J. A. Lopez-Sanchez, *Chin. J. Catal.*, 2016, **37**, 1619–1650.

203 B. K. Jena and C. R. Raj, *Langmuir*, 2007, **23**, 4064–4070.

204 S. Link and M. A. El-Sayed, *Int. Rev. Phys. Chem.*, 2000, **19**, 409–453.

205 C. G. Khoury and T. Vo-Dinh, *J. Phys. Chem. C*, 2008, 18849–18859.

206 P. Pallavicini, A. Donà, A. Casu, G. Chirico, M. Collini, G. Dacarro, A. Falqui, C. Milanese, L. Sironic and A. Tagliettia, *Chem. Commun.*, 2013, **49**, 6265–6267.

207 Y. Liu, K. Ma, T. Jiao, R. Xing, G. Shen and X. Yan, *Sci. Rep.*, 2017, **7**, 42978.

208 P. Vijayaraghavan, C.-H. Liu, R. Vankayala, C.-S. Chiang and K. C. Hwang, *Adv. Mater.*, 2014, **39**, 6689–6695.

209 Y. Liu, Z. Chang, H. Yuan, A. M. Fales and T. Vo-Dinh, *Nanoscale*, 2013, **5**, 12126–12131.

210 Q. Wu, Y. Sun, P. Ma, D. Zhang, S. Li, X. Wang and D. Song, *Anal. Chim. Acta*, 2016, **913**, 137–144.

211 S. Mariani, S. Scarano, J. Spadavecchia and M. Minunni, *Biosens. Bioelectron.*, 2015, **74**, 981–988.

212 R. Agarwal, V. Singh, P. Jurney, L. Shi, S. V. Sreenivasan and K. Roy, *Proc. Natl. Acad. Sci. U. S. A.*, 2013, **110**, 17247–17252.

213 Z. Y. Ong, S. Chen, E. Nabavi, A. Regoutz, D. J. Payne, D. S. Elson, D. T. Dexter, I. E. Dunlop and A. E. Porter, *ACS Appl. Mater. Interfaces*, 2017, **9**, 39259–39270.